AD NUMBER

AD846730

LIMITATION CHANGES

TO:

Approved for public release; distribution is unlimited.

FROM:

Distribution authorized to U.S. Gov't. agencies and their contractors; Critical Technology; JUN 1968. Other requests shall be referred to Air Force Rome Air Development Center, EMATE, Griffiss AFB, NY. This document contains export-controlled technical data.

AUTHORITY

radc, usaf, ltr, 17 sep 1971

RADC-TR-68-525
Final Report, 30 June 1968

STRIPLINE FERRITE DEVICES

Martin Sherman

Contractor: Syracuse University Research Corporation
Contract Number: F30602-67-C-0378
Effective Date of Contract: 1 June 1967
Contract Expiration Date: 1 June 1968
Amount of Contract: $52,550.00
Program Code Number: 7E30

Principal Investigator: Martin Sherman
Phone: 315-477-8495

Project Engineer: P. A. Romanelli
Phone: 315-330-4251

Sponsored by
Advanced Research Projects Agency
ARPA Order No. 550.

Rome Air Development Center
Air Force Systems Command
Griffiss Air Force Base, New York

STRIPLINE FERRITE DEVICES

Martin Sherman
Syracuse University Research Corporation

This research was supported by the Advanced Research Projects Agency of the Department of Defense and was monitored by P. A. Romanelli, RADC (EMATE), GAFB, N.Y. 13440 under Contract No. F30602-67-C-0378.

When US Government drawings, specifications, or other data are used for any purpose other than a definitely related government procurement operation, the government thereby incurs no responsibility nor any obligation whatsoever; and the fact that the government may have formulated, furnished, or in any way supplied the said drawings, specifications, or other data is not to be regarded, by implication or otherwise, as in any manner licensing the holder or any other person or corporation, or conveying any rights or permission to manufacture, use, or sell any patented invention that may in any way be related thereto.

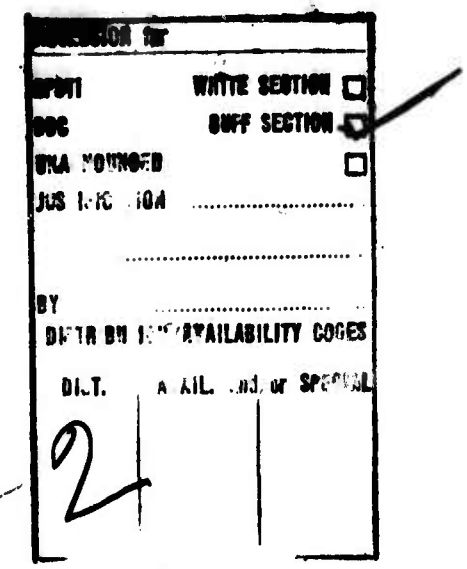

Do not return this copy. Retain or destroy.

FOREWORD

Distribution of this report is restricted under the provisions of the U.S. Mutual Security Acts of 1949.

Approved: Patsy A. Romanelli
PATSY A. ROMANELLI
Project Engineer
Electron Devices Section

Approved:
LEO W. SULLIVAN
Colonel, USAF
Chief, Surveillance and
Control Division

FOR THE COMMANDER
IRVING J. GABELMAN
Chief, Advanced Studies Group

ABSTRACT

A stripline instantaneous wideband nonreciprocal hybrid using ferrite material is described. A simple theory of operation, potential use as a broadband circulator and switch is described. The design and data on a laboratory model operating from 3 GHz to 9 GHz is presented.

The theory and results on a three-port switchable S-band microstrip circulator suitable for microwave integrated circuits is also reported. The circulator had a 2 db insertion loss and a 2% bandwidth. Although the insertion loss could be decreased by more refined etching and polishing techniques, the high Q inherent in this "ring" principle of operation severely limits the bandwidth.

RF sputtering process to deposit dielectric materials for obtaining thin film capacitors is also described.

EVALUATION

1. The purpose of this program was to develop stripline ferrite devices, and in particular a nonreciprocal wideband stripline hybrid and a three-port switchable S-band microstrip circulator were studied. The techniques of depositing dielectric materials to obtain thin film capacitors by RF sputtering was also to be investigated.

2. The report presents the theory, designs, and data for stripline hybrids in the 2 to 9 GHz frequency region. An S-band three-port circulator is also described. Data shows the frequency coverage is 2.40 to 2.45 GHz and insertion loss is 2.5 db.

3. RF sputtering process to deposit dielectric materials is described. Data regarding process is presented. Thin film capacitors were not made.

Patsy A. Romanelli

PATSY A. ROMANELLI
Project Engineer
Electron Devices Section

TABLE OF CONTENTS

LIST OF ILLUSTRATIONS

LIST OF ILLUSTRATIONS

SECTION 1

INTRODUCTION

A nonreciprocal wideband stripline hybrid using ferrite material is described. A simple theory of operation and its potential use as a broadband circulator and switch is described. The design data on a laboratory model operating from 3 GHz to 9 GHz is presented.

The theory and results on a three-port switchable S-band microstrip circulator suitable for microwave integrated circuits is also reported. The circulator had a 2 db insertion loss and a 2% bandwidth. Although the insertion loss could be decreased by more refined etching and polishing techniques, the high Q inherent in this "ring" principle of operation severely limits the bandwidth.

SECTION 2

GYROMAGNETIC HYBRID

2.1 Introduction

The gyromagnetic hybrid consists of two transmission lines which are brought into proximity with each other and with a ferrimagnetic material as indicated in Figure 1 . It utilizes the Faraday rotation phenomena that occurs in ferrimagnetic material to couple RF energy from one transmission line to the other. Any device based upon this principle is capable of attaining the large bandwidths normally associated with Faraday rotation.

The gyromagnetic hybrid functions as a nonreciprocal 180° 3 db hybrid. In its basic form it does not offer anything that cannot be obtained with a multi-section broadband 90° backward wave TEM coupler. However it forms the building block for many broadband devices. In conjunction with passive reciprocal networks or in cascade with another gyromagnetic hybrid it may be operated as a broadband (potentially multi-octave) circulator or switch.

The following sections discuss the basic theory, the hybrid characterization and device application, and the experimental results obtained on a laboratory model. The basic theory is presented in terms of normal modes[1, 2] rather than direct Faraday rotation[3].

2.2 Theory of Operation

Three coupling mechanisms exist in the coupled transmission line pair illustrated in Figure 1 . These will be referred to as (1) backward wave reciprocal coupling, (2) forward wave reciprocal coupling, and (3) gyromagnetic coupling. In designing a gyromagnetic hybrid it is necessary to choose a device geometry which eliminates or at least minimizes the backward and forward wave reciprocal coupling. The gyromagnetic hybrid operation and broad bandwidth are critically dependent upon the minimization of the undesirable reciprocal coupling mechanisms. Therefore, before discussing the

A5013

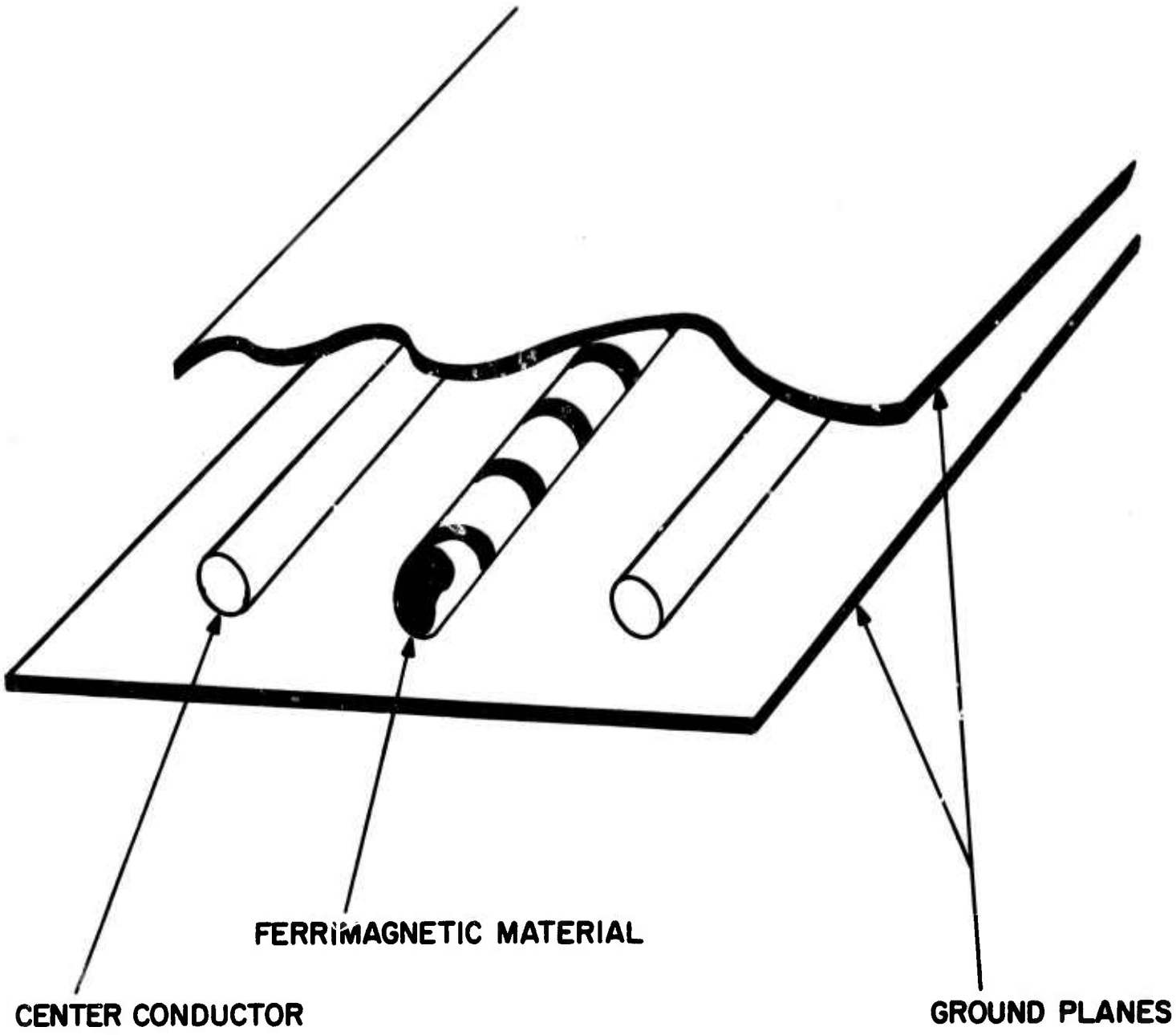

Figure 1. Basic Gyromagnetic Hybrid Configuration.

gyromagnetic coupling mechanism, discussion of reciprocal coupling is presented. To keep the presentation simple, each coupling mechanism is studied independently of the others even though in the physical device all coupling mechanisms may be present simultaneously.

The backward wave reciprocal coupling is caused by the mutual inductance and capacitance that exists between two TEM-mode coupled-transmission-lines[4]. The TEM-mode implies that the medium has a homogeneous dielectric constant so that any excitation of the transmission lines propagates with a velocity characteristic of the medium and independent of the geometry. The coupled voltage in a backward wave coupler which utilizes this coupling mechanism is given by

$$\frac{E_3}{A} = \frac{j\,k\,\sin\theta}{\sqrt{1-k^2}\,\cos\theta + j\sin\theta} \qquad (1)$$

and the output of the d.c. path is

$$\frac{E_2}{A} = \frac{\sqrt{1-k^2}}{\sqrt{1-k^2}\,\cos\theta + j\sin\theta} \qquad (2)$$

where

A = input voltage

θ = electrical length of coupled section

k = coupling factor.

The coupling factor is given by

$$k = \frac{Z_{oe} - Z_{oo}}{Z_{oe} + Z_{oo}} \qquad (3)$$

where

Z_{oe} = even mode impedance (+1, +1 excitation)

Z_{oo} = odd mode impedance (+1, -1, excitation)

The coupling obtained is periodic with frequency and attains its maximum value of k when θ is odd number of quarter-wavelengths. Also note the E_1 and E_4 are not zero unless

$$Z_o = \sqrt{Z_{oe} Z_{oo}} \tag{4}$$

where Z_o is the characteristic impedance of one transmission line with the other one removed. Thus, to minimize this coupling effect, Z_{oe} and Z_{oo} should be as nearly equal to Z_o as is practically possible. The separation between transmission lines (large separations imply $Z_{oo} \approx Z_{oe} \approx Z_o$) is limited by the necessity of obtaining gyromagnetic coupling in the actual device.

Reciprocal forward wave coupling occurs between two coupled transmission lines when the two normal mode velocities are unequal. This is possible for example, in strip transmission lines when the dielectric cross-section is inhomogeneous (two different dielectric constants or permeabilities for example). This situation exists in the gyromagnetic hybrid when the cross section is composed of high dielectric material, ferrimagnetic material, and teflon-fiberglass board. This coupling poses the most serious problem to broadband gyromagnetic hybrid operation. Whereas backward wave coupling reaches a maximum value periodically with frequency, forward wave reciprocal coupling increases with frequency until all the power is coupled over. Greatest consideration in the device cross-section must be given to minimizing this coupling.

Assuming that $Z_{oe} = Z_{oo} = Z_o$, the coupling in the device is given by (Figure 2)

$$\frac{E_2}{A} = -je^{-j\beta \ell} \sin\left(\frac{\Delta\beta}{2} \ell\right) \tag{5}$$

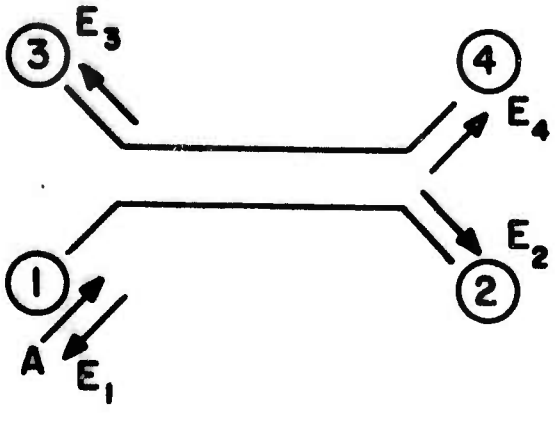

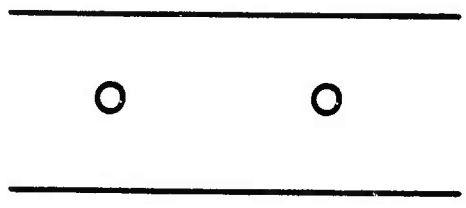

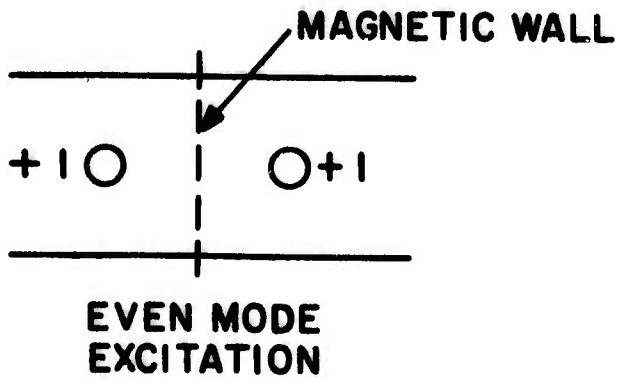

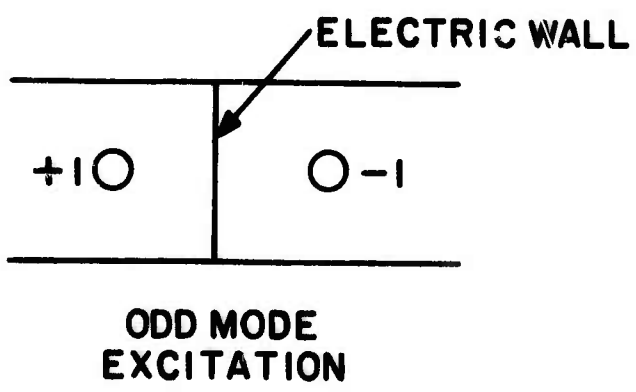

Figure 2. Coupled Transmission Lines

$$\frac{E_4}{A} = e^{-j\beta \ell} \cos\left(\frac{\Delta\beta}{2}\ \ell\right) \qquad (6)$$

where

$$\beta = \frac{\beta_e + \beta_o}{2}$$

$$\Delta\beta = \beta_e - \beta_o$$

$\beta_e = \frac{\omega}{v_e}$ = even mode propagation constant

$\beta_o = \frac{\omega}{v_o}$ = odd mode propagation constant

ℓ = length of coupled section

It is clearly necessary to equalize even and odd mode propagation velocities in the device.

When Z_{oe} and Z_{oo} are not equal to Z_o, some RF energy is reflected in port 1 and some comes out of port 3.

The gyromagnetic coupling is very similar to the forward wave reciprocal coupling in that it involves unequal normal mode propagation velocities. Figure 3 shows two coupled transmission lines embedded in ferrimagnetic material. The normal modes for this device are (1, j) and (1, -j). When ports 1 and 2 are excited with these modes, the coupled lines set up elliptically polarized fields in the medium with opposite sense of polarization on either side of the symmetry plane containing the two center conductors (Figure 3-b). This necessitates the opposite alignment of magnetic dipoles in the ferrimagnetic material. Each normal mode experiences a different permeability and therefore has a different propagation velocity. For equal normal mode impedances no RF energy is reflected at the excitation ports.

A5810

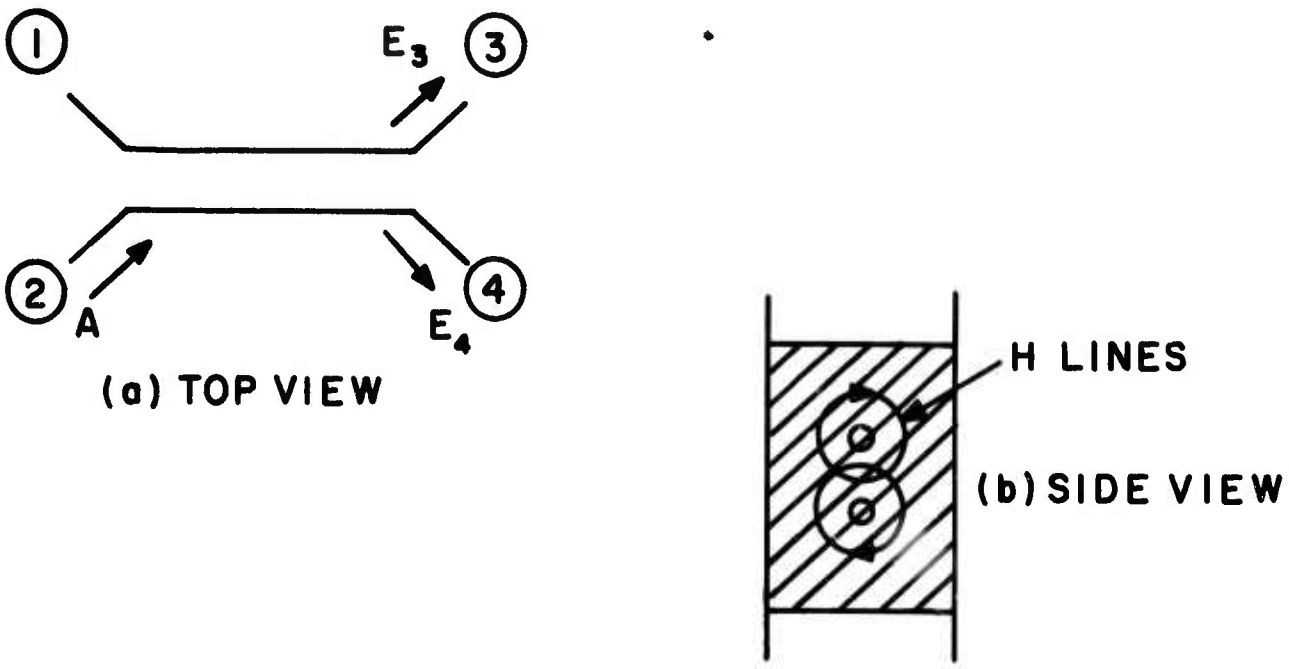

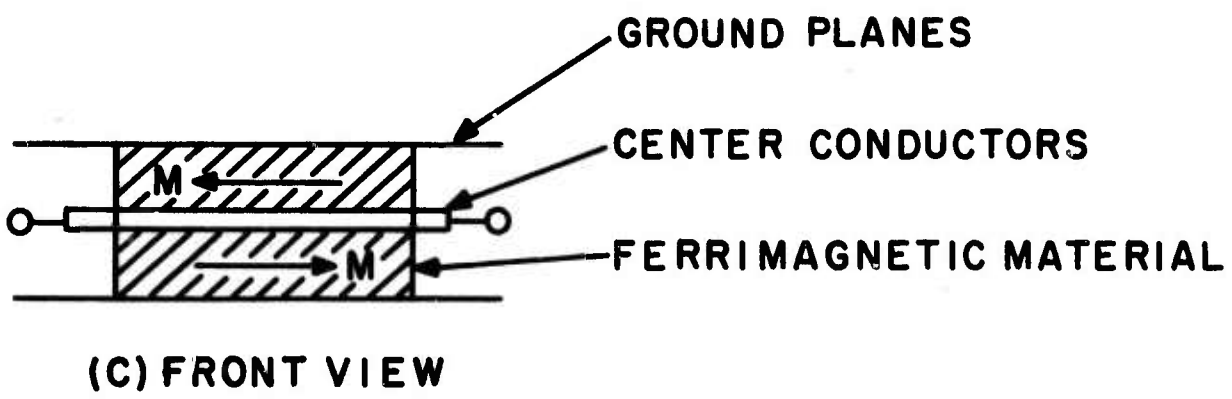

Figure 3.

Coupled Transmission Lines Imbedded in Ferrimagnetic Medium.

An excitation of unity at port 1 and zero at port 2 is equivalent to equal normal mode excitation.

$$\begin{pmatrix} 1 \\ 0 \end{pmatrix} = \frac{1}{2} \begin{pmatrix} 1 \\ -j \end{pmatrix} + \frac{1}{2} \begin{pmatrix} 1 \\ +j \end{pmatrix} \tag{7}$$

Defining the propagation constant for (1, -j) normal mode as β_1 and the (1, +j) normal mode as β_2, the output at ports 3 and 4 are

$$\begin{pmatrix} E_3 \\ E_4 \end{pmatrix} = \frac{1}{2} \begin{pmatrix} e^{-j\beta_1 \ell} \\ -je^{-j\beta_1 \ell} \end{pmatrix} + \frac{1}{2} \begin{pmatrix} e^{-j\beta_2 \ell} \\ +je^{-j\beta_2 \ell} \end{pmatrix} \tag{8}$$

or,

$$E_3 = e^{-j\theta} \cos \Delta\phi$$

$$E_4 = e^{-j\theta} \sin \Delta\phi$$

where

$\Delta\phi = \frac{1}{2}(\beta_2 - \beta_1)\ell$ = one half the nonreciprocal phase shift

$\theta = \frac{1}{2}(\beta_2 + \beta_1)\ell$ = the average insertion phase

Applying unit excitation to each port, the scattering matrix is determined as

$$S^1 = e^{-j\theta} \left[\begin{array}{cc|cc} 0 & 0 & \cos \Delta\phi & -\sin\Delta\phi \\ 0 & 0 & \sin \Delta\phi & \cos \Delta\phi \\ \hline \cos \Delta\phi & -\sin\Delta\phi & 0 & 0 \\ \sin \Delta\phi & \cos \Delta\phi & 0 & 0 \end{array}\right] \tag{9}$$

where the superscript 1 indicates the assumed magnetic dipole alignment. Notice that the nonreciprocal nature of the device in the negative sign before the sin $\Delta\phi$ term. For the opposite magnetic dipole alignment (superscript 2),

the scattering matrix is

(equation 10)

$$S^2 = \tilde{S}^1 = e^{-j\theta} \left[\begin{array}{cc|cc} 0 & 0 & \cos\Delta\phi & \sin\Delta\phi \\ 0 & 0 & -\sin\Delta\phi & \cos\Delta\phi \\ \cos\Delta\phi & \sin\Delta\phi & 0 & 0 \\ -\sin\Delta\phi & \cos\Delta\phi & 0 & 0 \end{array}\right]$$

the transpose of state 1. This completely characterizes the ideal gyromagnetic coupler.

2.3 Basic Devices

The gyromagnetic hybrid is obtained when the differential phase shift is 90° ($\Delta\phi = 45°$) resulting in

$$S^1 = \tilde{S}^2 = \frac{1}{\sqrt{2}} e^{-j\theta} \left[\begin{array}{cc|cc} 0 & 0 & 1 & -1 \\ 0 & 0 & -1 & -1 \\ 1 & -1 & 0 & 0 \\ -1 & 1 & 0 & 0 \end{array}\right] \qquad (11)$$

It is a nonreciprocal 180° 3 db hybrid (nonreciprocal magic T) with an insertion phase θ. It is instructive to compare this with a reciprocal magic T which has a scattering matrix

$$S^R = \frac{1}{\sqrt{2}} \left[\begin{array}{cc|cc} 0 & 0 & 1 & 1 \\ 0 & 0 & 1 & -1 \\ 1 & 1 & 0 & 0 \\ 1 & -1 & 0 & 0 \end{array}\right] \qquad (12)$$

in which ports 2 and 4 are the Δ ports and ports 1 and 3 are the Σ ports. On comparing these two scattering matrices it is evident that the gyromagnetic hybrid functions like a magic T with a gyrator (180° nonreciprocal phase shift) in each Δ port as indicated in Figure 4-a. In state 2 the gyrators are interchanged.

Other devices are:

Three-Port Circulator

If two ports of the gyromagnetic hybrid are connected together by a simple T (Figure 4-b) the device becomes a three-port circulator. Power into port 1 divides equally between ports 3 and 4 with voltages in phase. The outputs from ports 3 and 4 therefore seem in the T junction and proceed out the transmission line. Power incident to the T from the transmission line divides equally to ports 3 and 4 with the voltages in phase and proceeds through the hybrid to sum at port 2. Power into port 2 divides equally to ports 3 and 4 with the voltages in anti-phase. The voltages are therefore reflected back into the hybrid by the T junction and sum at port 1. The device is thus a circulator. Reversing the magnetic state of the hybrid reverses the circulation direction. This device can be used as a single-pole/double-throw switch which has been reported in the literature[5]. A broadband T junction has also been discussed in the literature [6] so that a broadband three-port circulator is feasible.

Four-Port Circulator

Connecting ports 3 and 4 together with a magic T (Figure 4-c) the device becomes a four-port circulator. It can be used as a double pole/double-throw switch. This device has one path with a 180° phase difference relative to the other three paths.

Double-Pole/Double-Throw Switch (Equal Insertion Phase)

Connecting two hybrids back to back realizes a DPDT switch. By independently controlling the state of each hybrid it is possible to channel power from either of the input ports to either of the output ports with equal insertion phase.

A5012

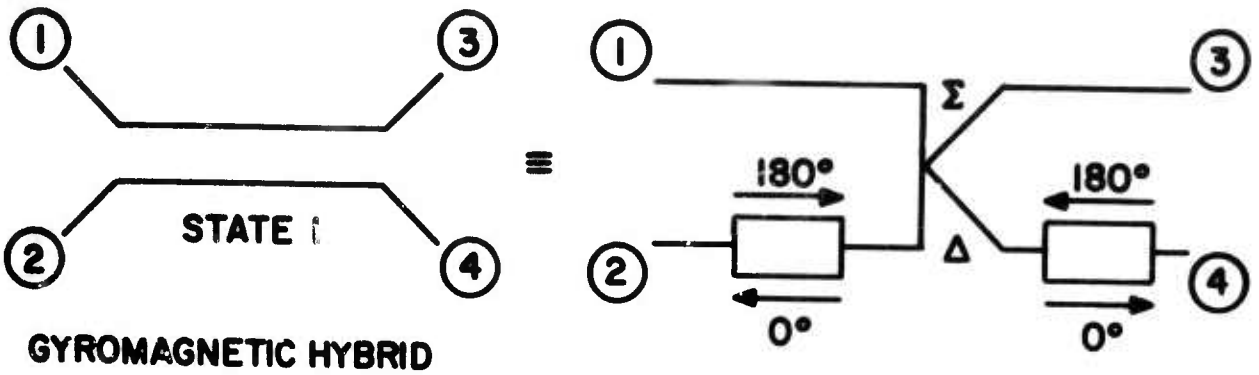

(a) GYROMAGNETIC HYBRID

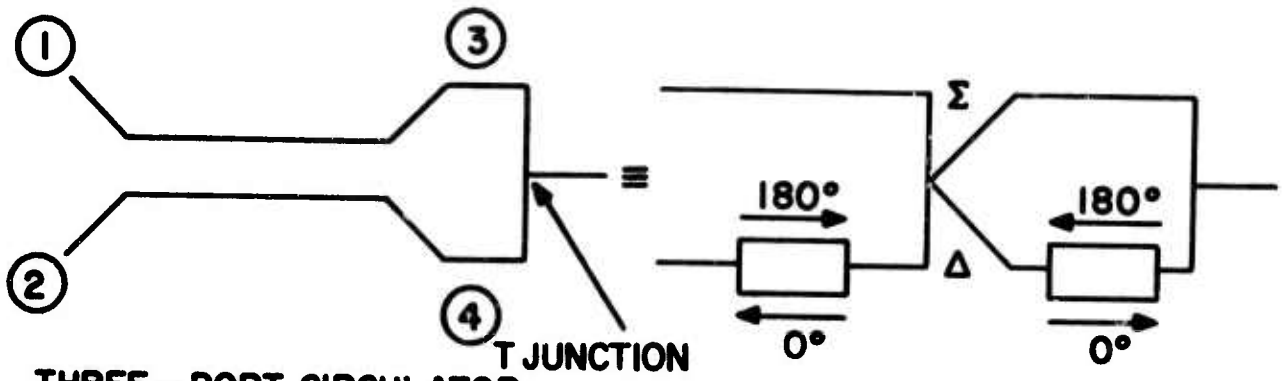

(b) THREE – PORT CIRCULATOR

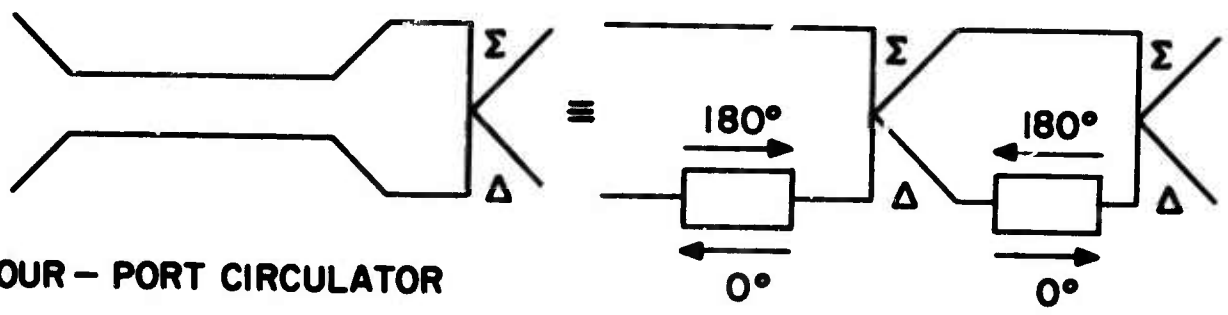

(c) FOUR – PORT CIRCULATOR

Figure 4. Gyromagnetic Devices.

2.4 Experimental Design

Placing ferrimagnetic material both above and below the center conductors of the coupled transmission lines requires the material be opposite magnetization in each half of the structure. This complicates the d.c. biasing problem[5]. It was therefore decided to half-load the structure with ferrimagnetic material so that an external coil could be used to supply H_{dc}. No attempt was made to minimize the ferrite cross-sectional area.

Flux plotting techniques on resistance paper were used to estimate the quantity and location of the circulator polarization. The coupled line spacing, S, was varied. The line width, W, was adjusted to give a 50 ohm system in a medium with a relative dielectric constant of 9. Sidewalls were not included. The unnormalized results are shown in Figure 5 . Because of the fear of moding and the neglected sidewalls a spacing of $S/b \approx .5$ was chosen. This is approximately 20db of backward wave coupling.

It was feared that the unsymmetrical ferrite loading would cause difficulty in obtaining the equal even and odd mode propagation velocities which is necessary for the elimination of the forward wave reciprocal coupling. This fear was not unfounded as much difficulty was encountered.

Several ferrite half-loaded cross-sections were tested (Figure 6). All were 1/2" wide and approximately 1/4" high. The exact heights may be determined from the figure. Five mil thick Copper-clad Mylar was included on the top and bottom to ensure good contact with the case and allow for a few mils compression. The coupled lines were etched on a 9 mil thick teflon-fiberglass board. A thinner board would decrease the undesirable coupling problem. However because some difficulty was encountered in handling the thin mylar sheets, the 9 mil teflon-fiberglass was used. This difficulty can certainly be overcome and should result in a decreased forward wave reciprocal coupling sensitivity to hybrid cross-section. The ferrite material is TT1-414 (Trans-Tech) which is specified with $\epsilon_r \approx 11$. D-13 material (Trans-Tech) with a nominal $\epsilon_r = 13$ was always used in the other half

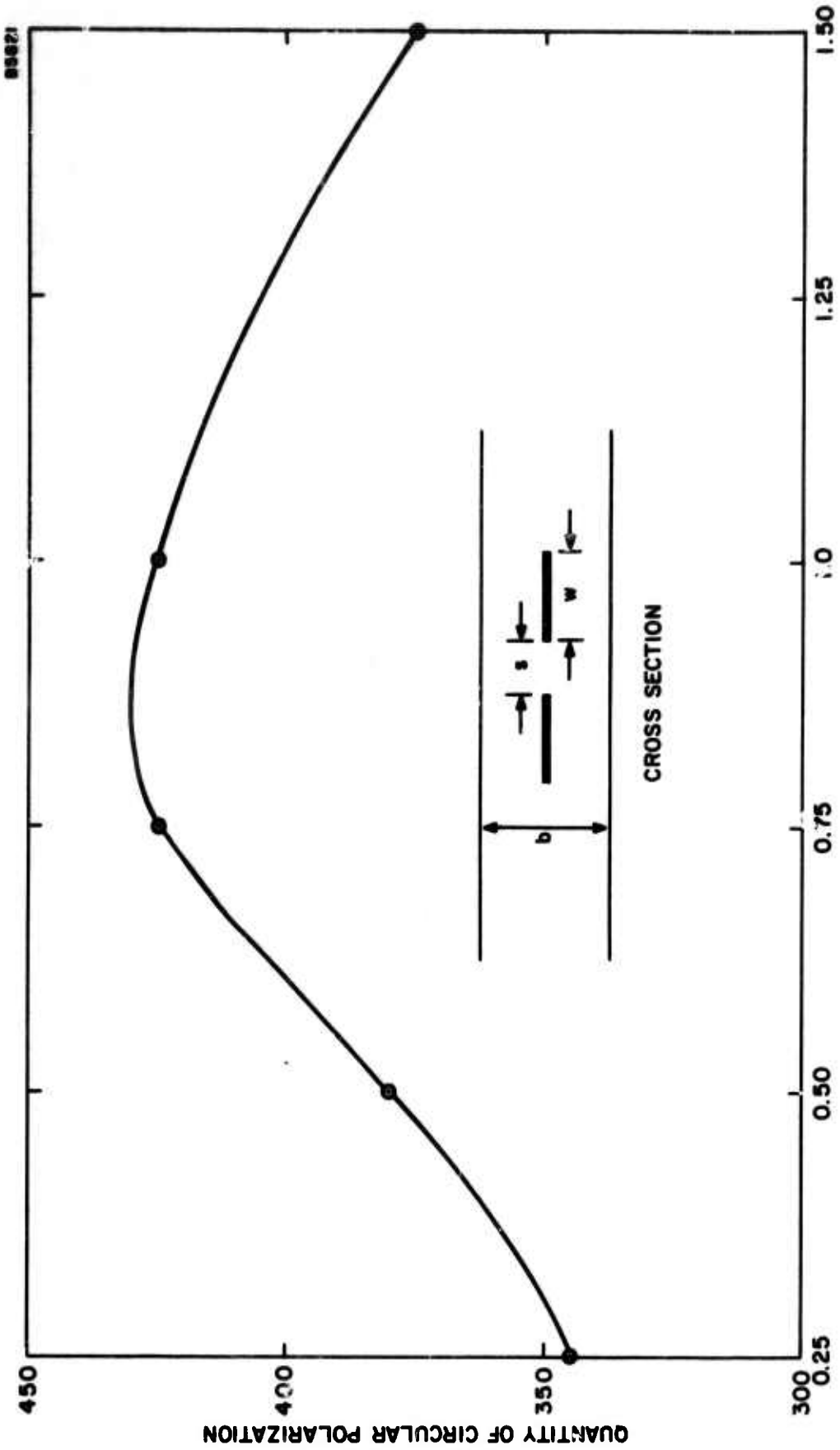

Figure 5. Circular Polarization vs. Geometry.

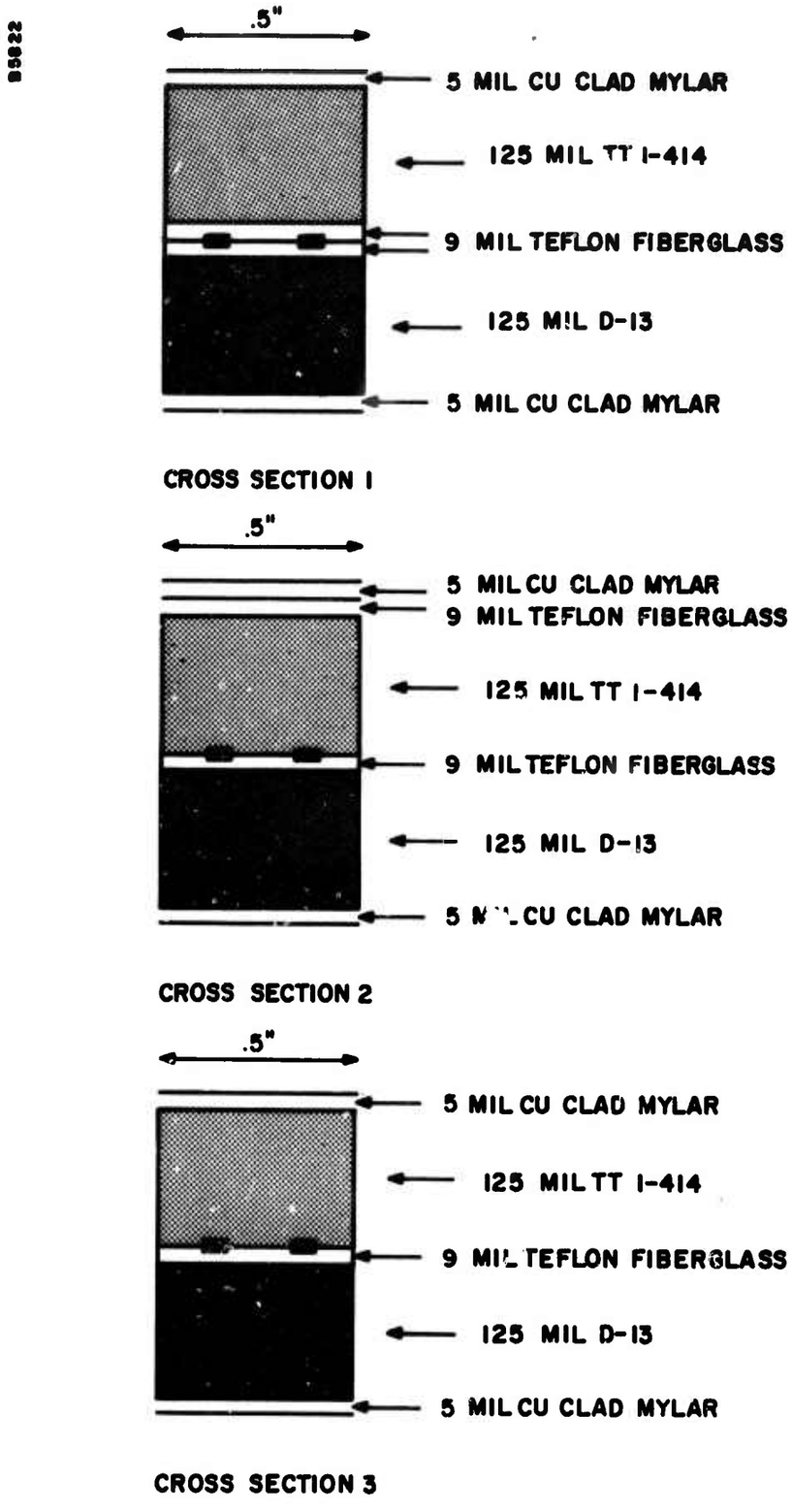

Figure 6. Cross-Sections for the Gyromagnetic Hybrid.

of the cross section. The coupled line length was 6". A photograph of the device is shown in Figure 7.

Figure 8 shows the forward wave reciprocal coupling present in cross-section #1. To simplify the evaluation of the effect of the 18 mil center section of teflon-fiberglass, the ferrite material was replaced by another slab of D-13. No attempt was made to match impedances. Replacing one slab of D-13 with TTI-414 had negligible effect on the coupling (Figure 9) outside the ferrite loss region. Increasing the separation between coupled lines from 60 mils to 120 mils decreased the coupling but did not eliminate it. (Figure 10) Eliminating one of the 9 mil teflon-fiberglass boards (cross-section #3) decreased the coupling still further but not nearly enough (Figure 11).

Finally, the unsymmetrical cross-section #2 was tested. The data indicated that the power out the forward wave coupling port was approximately 20 db down from the input power at frequencies up to 12 GHz.

Using this cross section and a coil with a measured axis field strength (without the hybrid inside) of 60 Oersted at the ends and 100 Oersted at the center, the smoothed results shown in Figure 12 were obtained. The coupled lines were 80 mils wide with a 120 mil separation. The width should probably be narrower to obtain a 50 ohm impedance. A more precise presentation of the data is shown in Figures 13 and 14 . The hybrid operated from 3 GHz to approximately 9 GHz. The lower frequency limit is set by the ferrite material domain wall resonances and the attendent losses. The upper limit in this case was set by erratic insertion loss spikes caused by either air gaps or more probably higher order stripline or waveguide modes. Reciprocal forward wave coupling was most definitely the limiting factor with this cross-section.

2.5 Conclusions

The minimization of the undesirable forward wave coupling at frequencies up to 12.4 GHz demonstrates the feasibility of obtaining multi-octave in-

5539

a)

b)

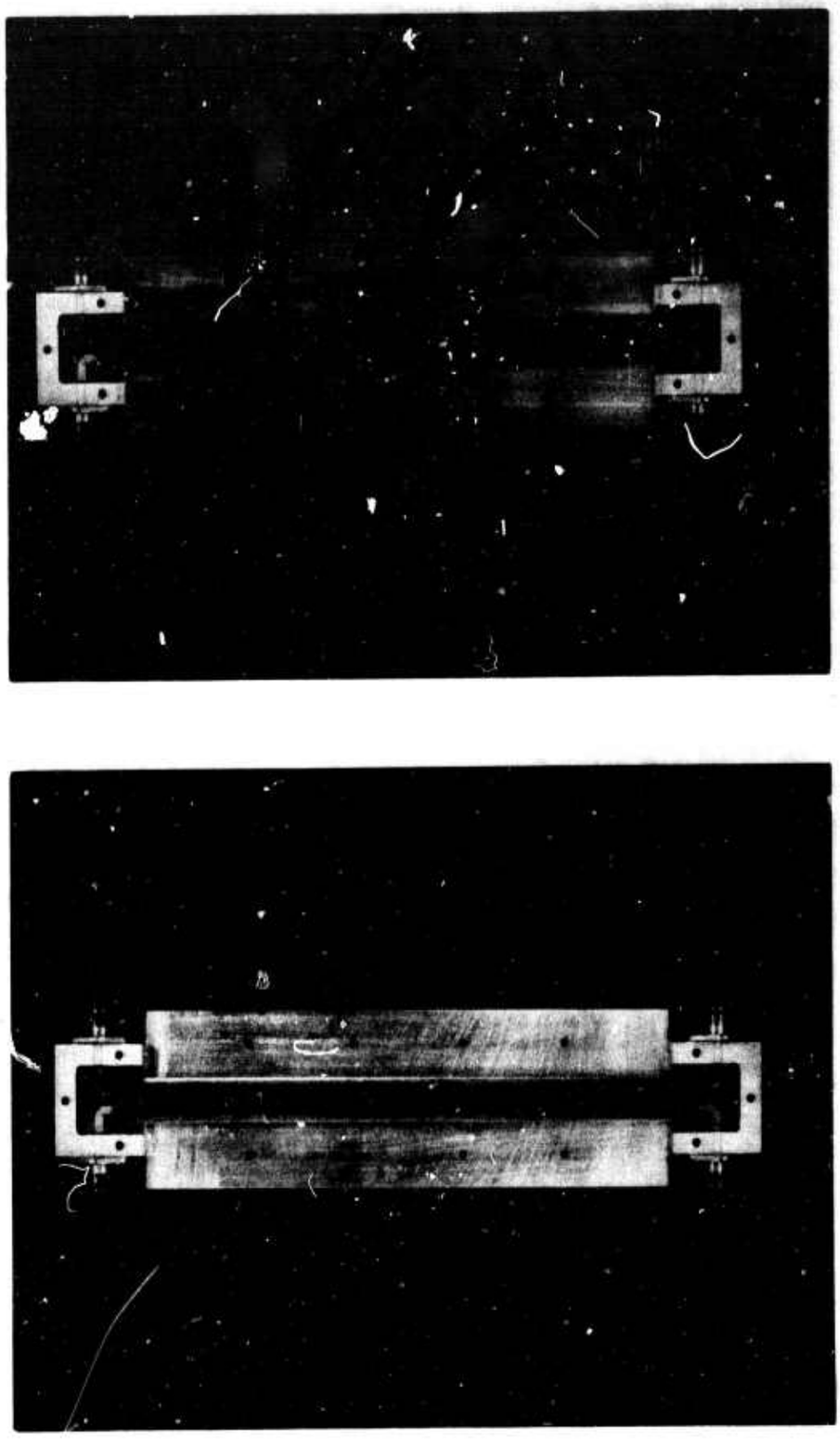

Figure 7. Four-Port Gyromagnetic Coupler.

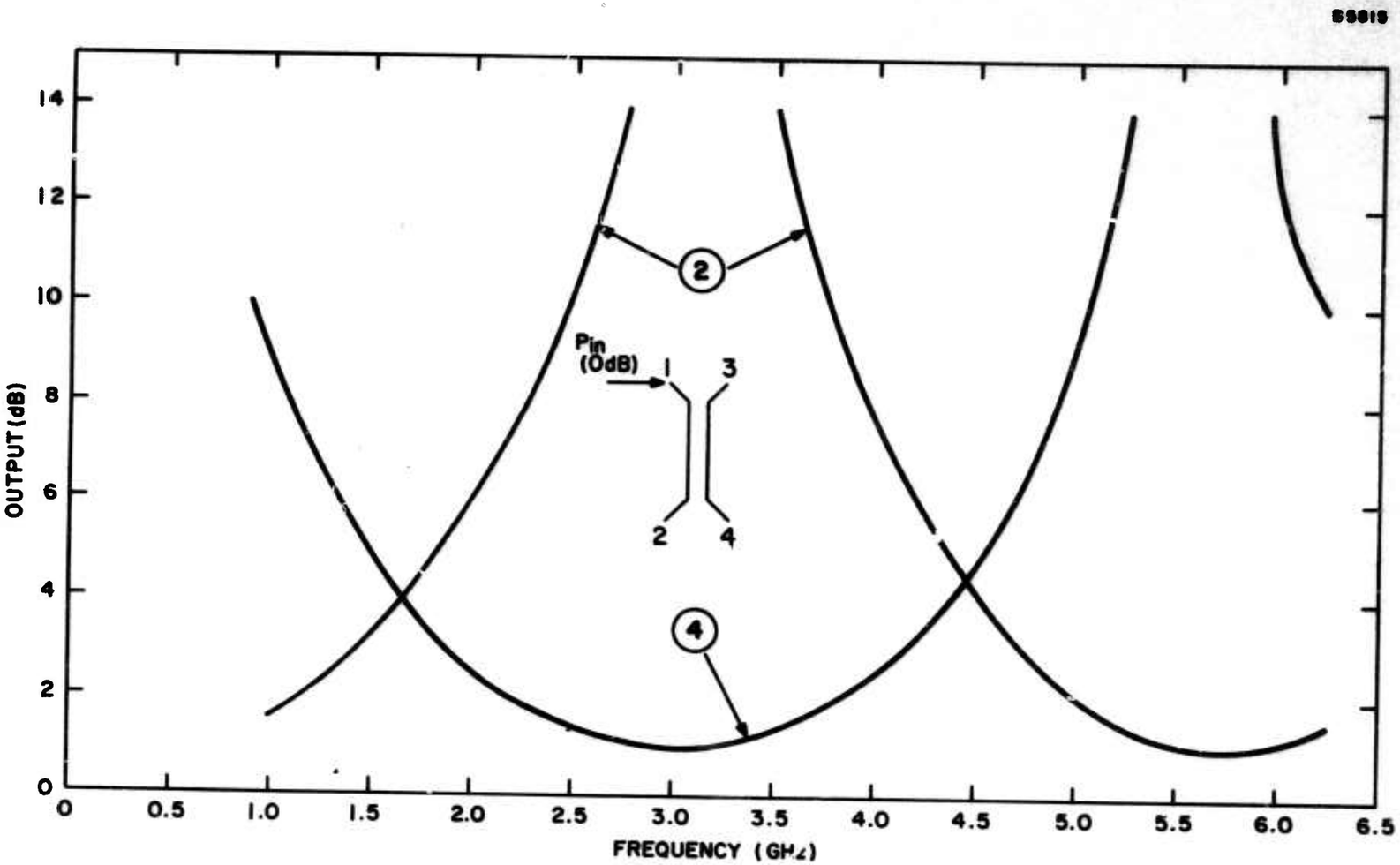

Figure 8. Reciprocal Coupling in Cross-Section #1
(All D-13, W = .030", S = .060")

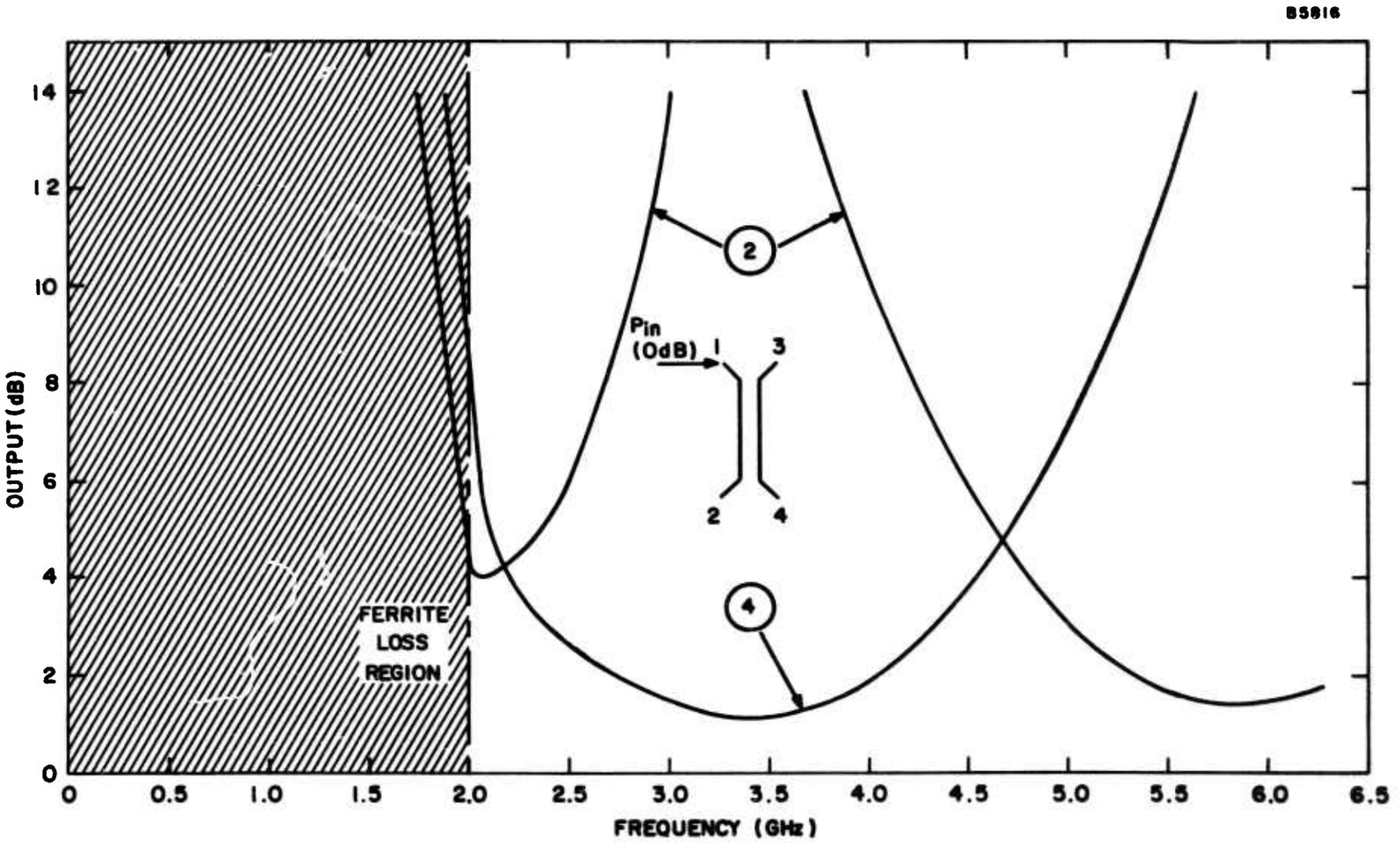

Figure 9. Reciprocal Coupling in Cross-Section #1
(D-13 and TT 1-414, W = .030", S = .060")

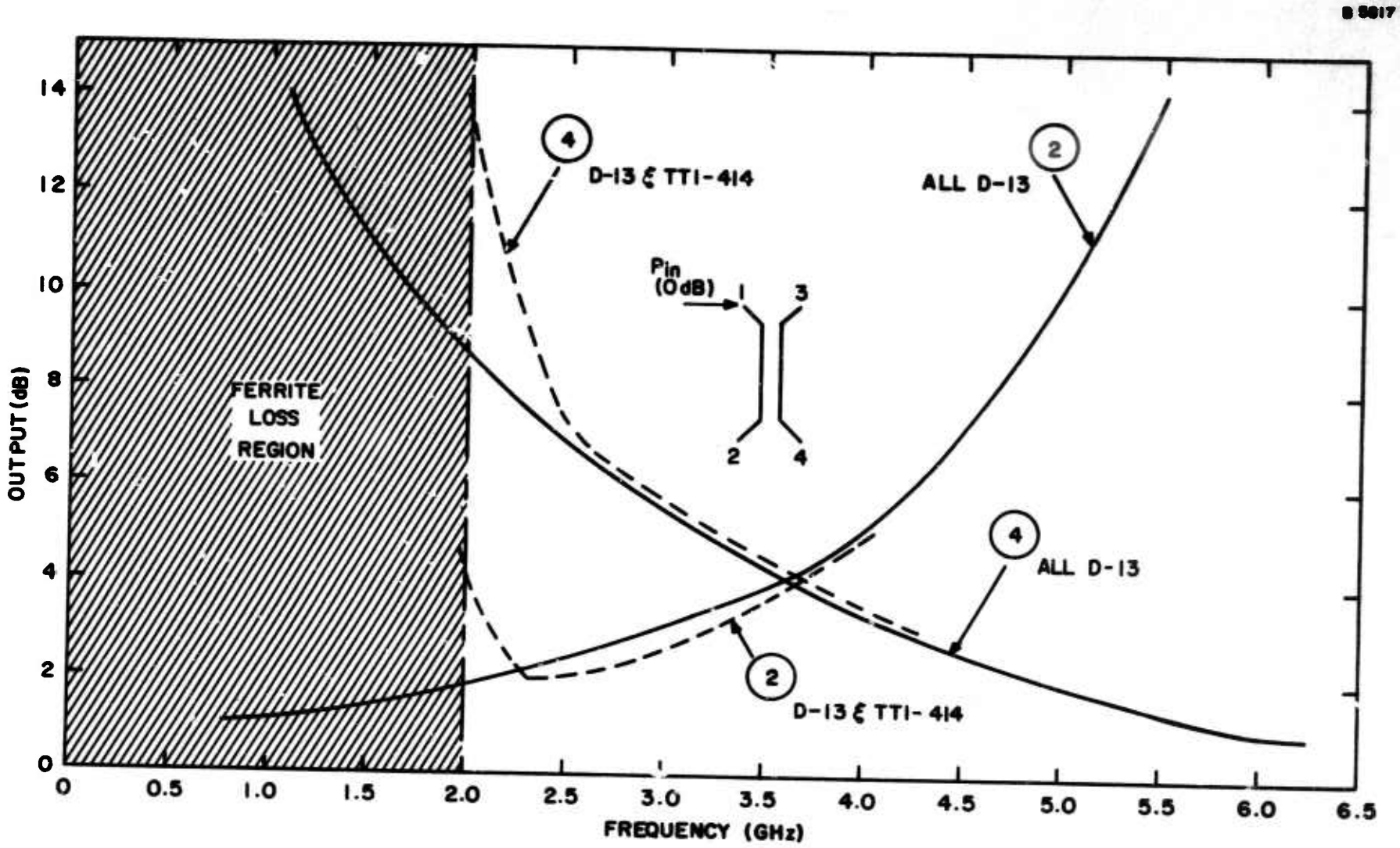

Figure 10. Reciprocal Coupling in Cross-Section #1 (W = .030", S = .120")

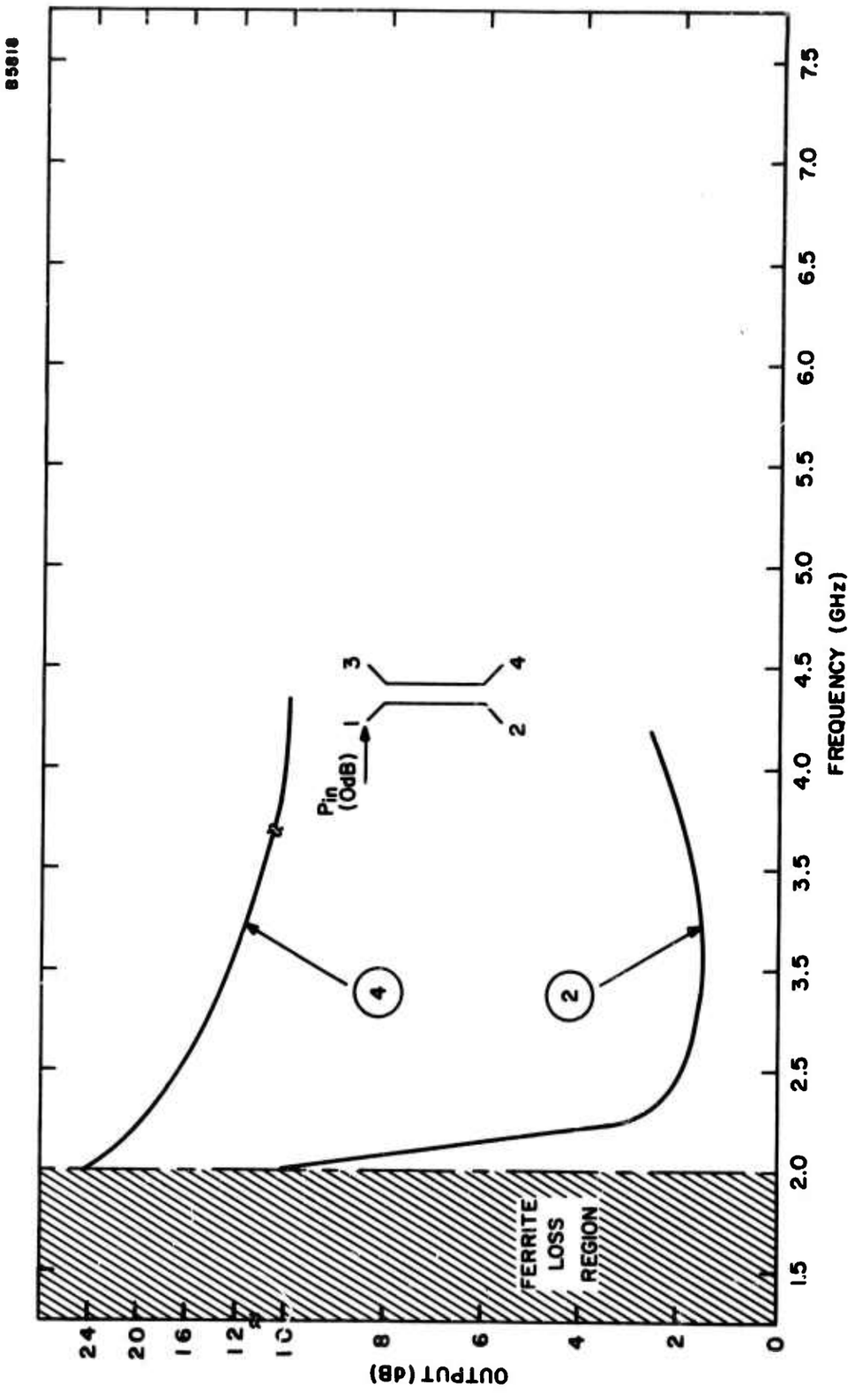

Figure 11. Reciprocal Coupling in Cross-Section #3
(W = .030", S = .120")

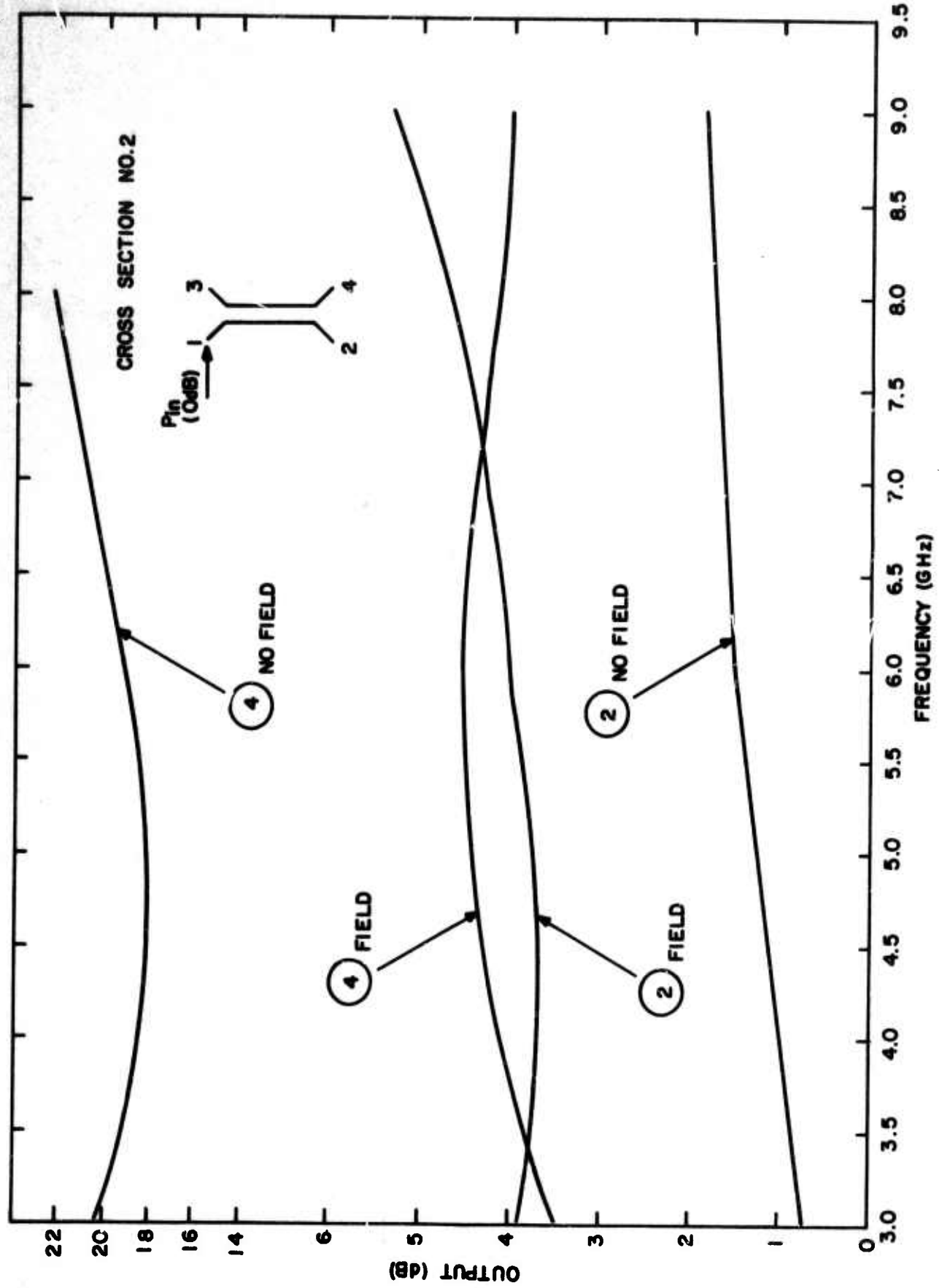

Figure 12. Gyromagnetic Hybrid Data, (3 GHz - 9 GHz).

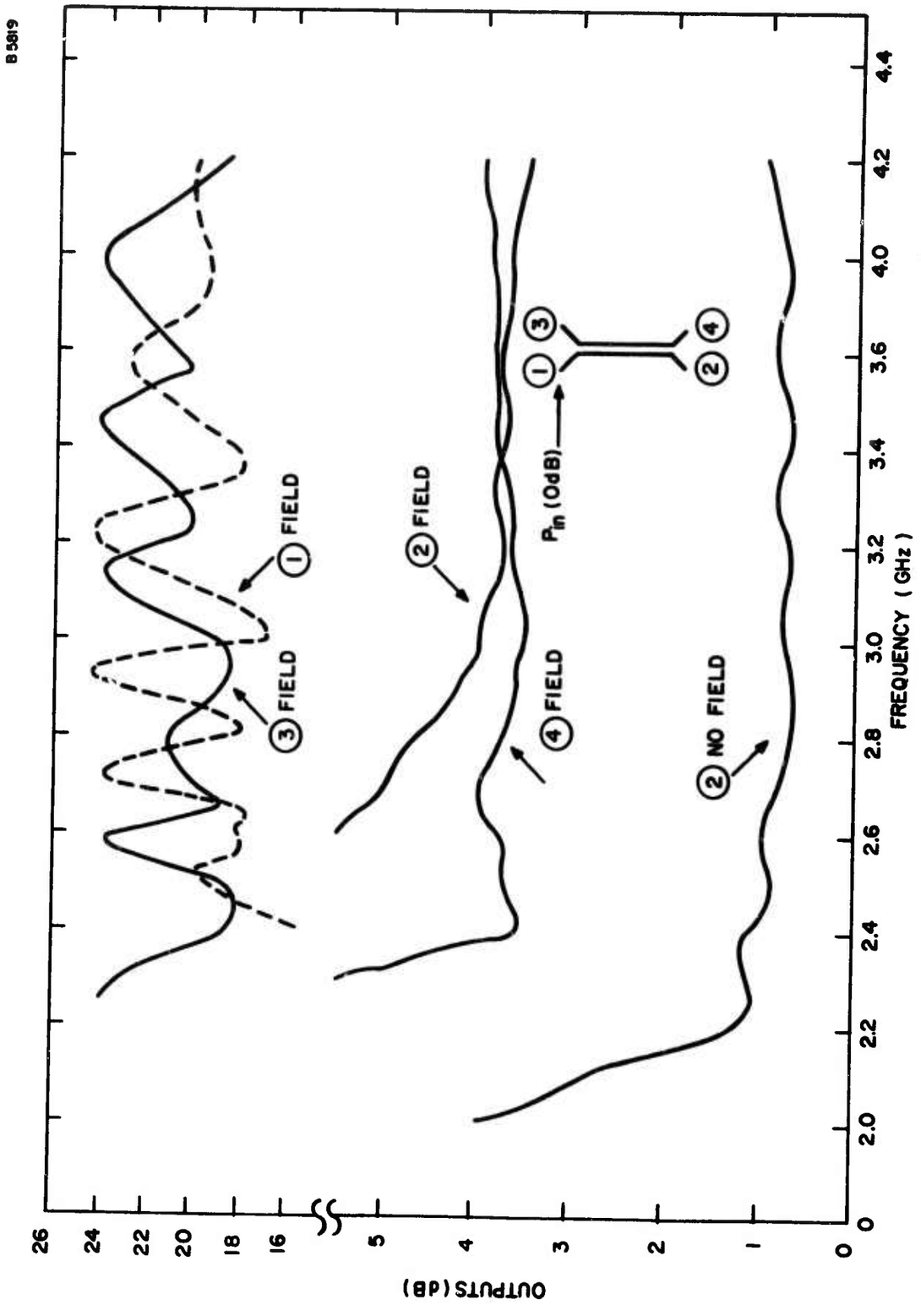

Figure 13. Gyromagnetic Hybrid Data, (2 GHz - 4 GHz).

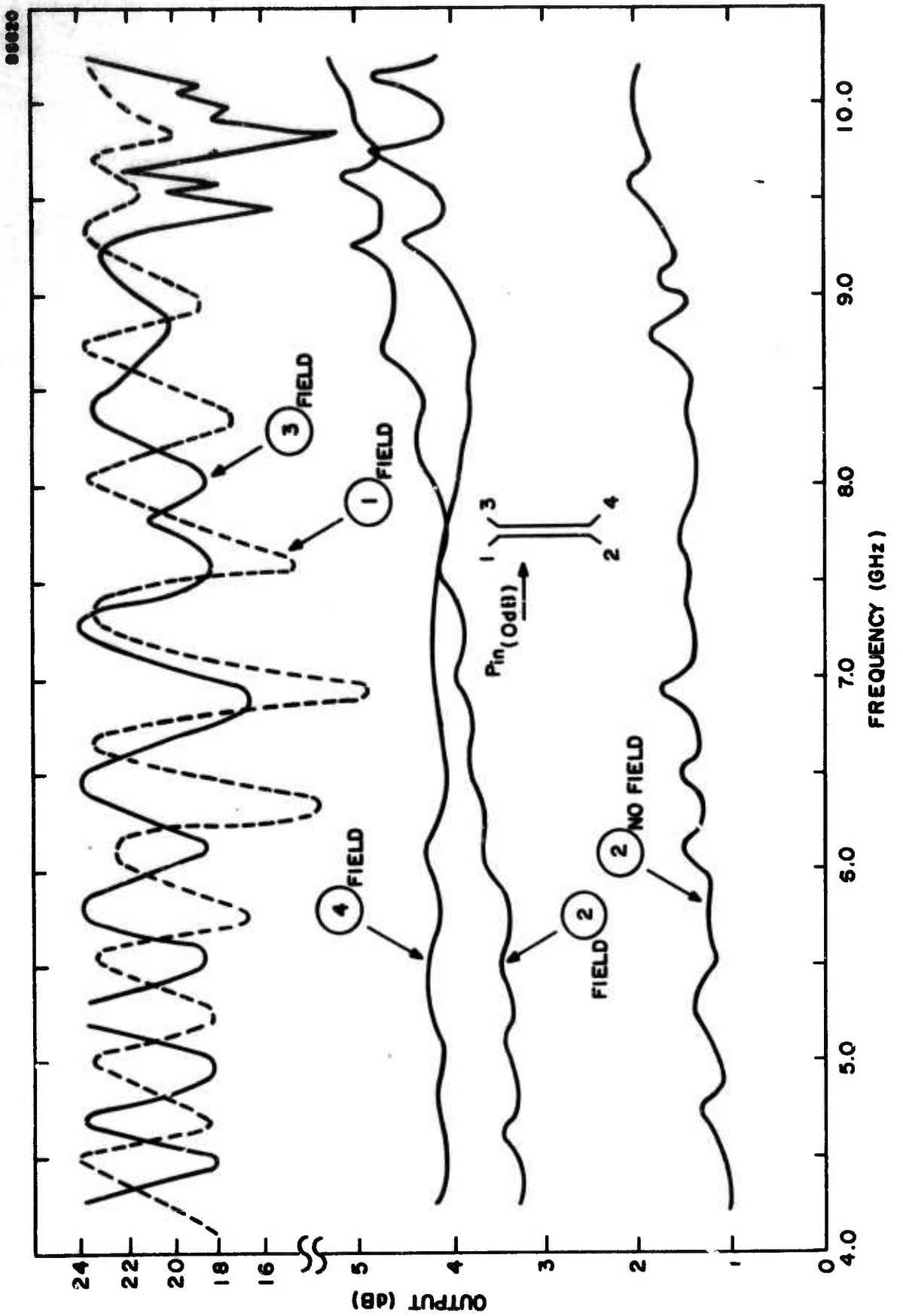

Figure 14. Gyromagnetic Hybrid Data, (4 GHz - 9 GHz).

stantaneous bandwidths with the gyromagnetic hybrid. A more accurate flux plotting evaluation of field conditions together with more accurately matched impedances should improve VSWR, isolation and amplitude balance, all of which are necessary for the realization of the broadband devices utilizing the gyromagnetic hybrid as a building block.

SECTION 3

RING CIRCULATOR

3.1 Introduction

This section describes the theory and experimental results obtained for an S-Band microstrip three-port ring circulator. The device was constructed from three meander line non-reciprocal phase shifters which were tied together in a ring by three tee-junctions. The circuit was deposited on a 20 mil thick ferrite disc. A switching wire runs through a hole in the center of the disc and the device is operated in a self-latching mode. The primary reasons for choosing this geometry were its low manufacturing cost and its compatability with microwave integrated circuits.

The initial circulator that was designed had a 2 db insertion loss and a bandwidth of approximately 2%. Attempts were made to increase the bandwidth by varying various meander line phase shifter parameters. All the devices tested had band widths of approximately 2%.

An analysis of the device shows that it has a high Q caused by the large insertion phases (of the phase shifters) required to obtain the required amount of non-reciprocal phase shift. Holding currents or permanent magnets rather than latching operation could increase the bandwidth. It appears doubtful that bandwidths of greater than a few percent can be obtained from the ring configuration.

3.2 Analysis

The scattering parameters of the ring circulator are related to the normal mode reflection coefficients by

$$S_{11} = \frac{1}{3}(s_1 + s_2 + s_3)$$

$$S_{21} = \frac{1}{3}(s_1 + e^{-j\gamma} s_2 + e^{+j\gamma} s_3) \qquad (13)$$

$$S_{31} = \frac{1}{3}(s_1 + e^{+j\gamma} s_2 + e^{-j\gamma} s_3)$$

where

S_{11} is the circulator reflection coefficient

S_{21}, S_{31} are the circulator transmission coefficients

s_1 is the zero rotation (1, 1, 1) normal mode reflection coefficient

s_2 is the positive rotation (1, $e^{-j\gamma}$, $e^{+j\gamma}$) normal mode reflection coefficient

s_3 is the negative rotation (1, $e^{+j\gamma}$, $e^{-j\gamma}$) normal mode reflection coefficient

γ $= 2\pi/3$

The ring circulator performance can be analyzed by finding its normal mode reflection coefficients.

A model for the three-port non-reciprocal ring circuit is shown in Figure 15. The ring circuit segments between the ports are non-reciprocal transmission lines. This is the limiting case of ideal non-reciprocal phase-shifters with perfect match and no loss. The parameters characterizing the circuit are indicated in the figure and are defined below:

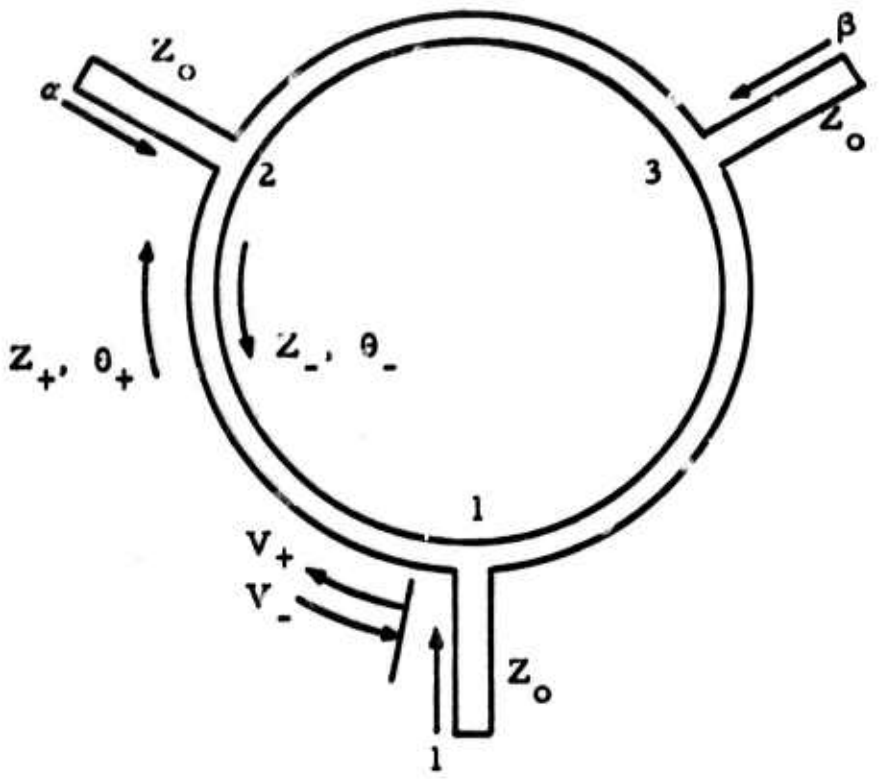

Figure 15. Circuit for Determining Reflection Coefficients of the Three-Port Ring Circulator.

Z_o: the characteristic impedance of each of the input ports to the ring

Z_+, Z_-: the characteristic impedance of the ring in the clockwise and counter-clockwise direction respectively.

θ_+, θ_-: the insertion phase in the clockwise and counter-clockwise directions, respectively, between any two adjacent ports.

Referring again to Figure 15, the ring circuit is assumed excited by its normal modes. For the even zero rotation modes:

$$\alpha = \beta = 1 \tag{14}$$

For the positive rotation mode:

$$\alpha = e^{-j2\pi/3} \quad \beta = e^{+j2\pi/3} \tag{15}$$

For the negative rotation mode:

$$\alpha = e^{+j2\pi/3} \quad \beta = e^{-j2\pi/3} \tag{16}$$

The total voltage V at port (1) is:

$$V = 1 + e^{j\phi} = V_+ + V_- \tag{17}$$

where ϕ is the angle of the voltage reflection coefficient

V_+, V_- are the total travelling waves in the ring circuit in the clockwise and counter-clockwise direction, respectively, immediately to the left of port (1).

The symmetrical component reflection coefficients is of unit magnitude for the lossless circuit. We desire an expression for ϕ.

The total current I flowing into port (1) is:

$$I = \frac{1-e^{j\phi}}{Z_o} = \frac{V_+}{Z_+} - \frac{V_-}{Z_-} - \beta \left(\frac{V_+}{Z_+} e^{-j\theta_+} + \frac{V_-}{Z_-} e^{+j\theta_-} \right) \tag{18}$$

The second term on the right side of this equation follows from the relationship between the device symmetry and the normal modes. It represents the current flowing into the junction from the ring segment to the right of the junction.

The voltage equation at port (2) is:

$$\alpha(1 + e^{j\phi}) = V_+ e^{-j\theta_+} + V_- e^{+j\theta_-} \tag{19}$$

Solving equations (17) and (19) yields:

$$V_+ = \frac{(1+e^{j\phi})(\alpha - e^{+j\theta_-})}{(e^{-j\theta_+} - e^{+j\theta_-})}$$

$$V_- = \frac{(1+e^{j\phi})(e^{-j\theta_+} - \alpha)}{(e^{-j\theta_+} - e^{+j\theta_-})} \tag{20}$$

It is convenient to express the insertion phase θ_+ and θ_- in terms of the average insertion phase θ and one-half the differential phase-shift ϵ:

$$\theta = \frac{\theta_- + \theta_+}{2}$$

$$\epsilon = \frac{\theta_- - \theta_+}{2} \tag{21}$$

or equivalently

$$\theta_- = \theta + \epsilon$$

$$\theta_+ = \theta - \epsilon \tag{22}$$

We also define

$$Z = 2\,\frac{Z_+ Z_-}{Z_+ + Z_-} \tag{23}$$

Using these parameters and substituting equations (20) into equation (17) gives:

$$\phi = 2 \tan^{-1} \left\{ \frac{2Z_o}{Z} \left[\frac{\cos\theta - \frac{1}{2}(\alpha e^{-j\epsilon} + \beta e^{j\epsilon})}{\sin\theta} \right] \right\} \qquad (24)$$

Inserting the values of α and β corresponding to the normal modes we finally obtain the expressions for the reflection coefficients. These are:

(1) Even Zero Rotation Mode

$$\phi_e = 2 \tan^{-1} \left\{ \frac{2Z_o}{Z} \left[\frac{\cos\theta - \cos\epsilon}{\sin\theta} \right] \right\} \qquad (25)$$

(2) Positive Rotation Mode

$$\phi_+ = 2 \tan^{-1} \left\{ \frac{2Z_o}{Z} \left[\frac{\cos\theta + \sin(30^\circ + \epsilon)}{\sin\theta} \right] \right\} \qquad (26)$$

(3) Negative Rotation Mode

$$\phi_- = 2 \tan^{-1} \left\{ \frac{2Z_o}{Z} \left[\frac{\cos\theta + \sin(30^\circ + \epsilon)}{\sin\theta} \right] \right\} \qquad (27)$$

The reference planes for these reflection coefficients are at the three junctions of the ring and input ports.

The ring circulates when the three normal mode reflection coefficients are mutually separated by 120°. The three reflection coefficients are plotted in Figure 16 for a ring impedance Z_o of 50 ohms and a non-reciprocal phase shift 2ϵ of 60°. The abscissa is the average insertion phase of the non-reciprocal phase shifter between the tee-junctions. For these values of impedance and phase shift the ring circulates when the average $(\theta_+ + \theta_-/2)$ electrical length of the phase shifter is an odd number of quarter wavelengths.

A formula for the bandwidth is obtained by taking the variation, about

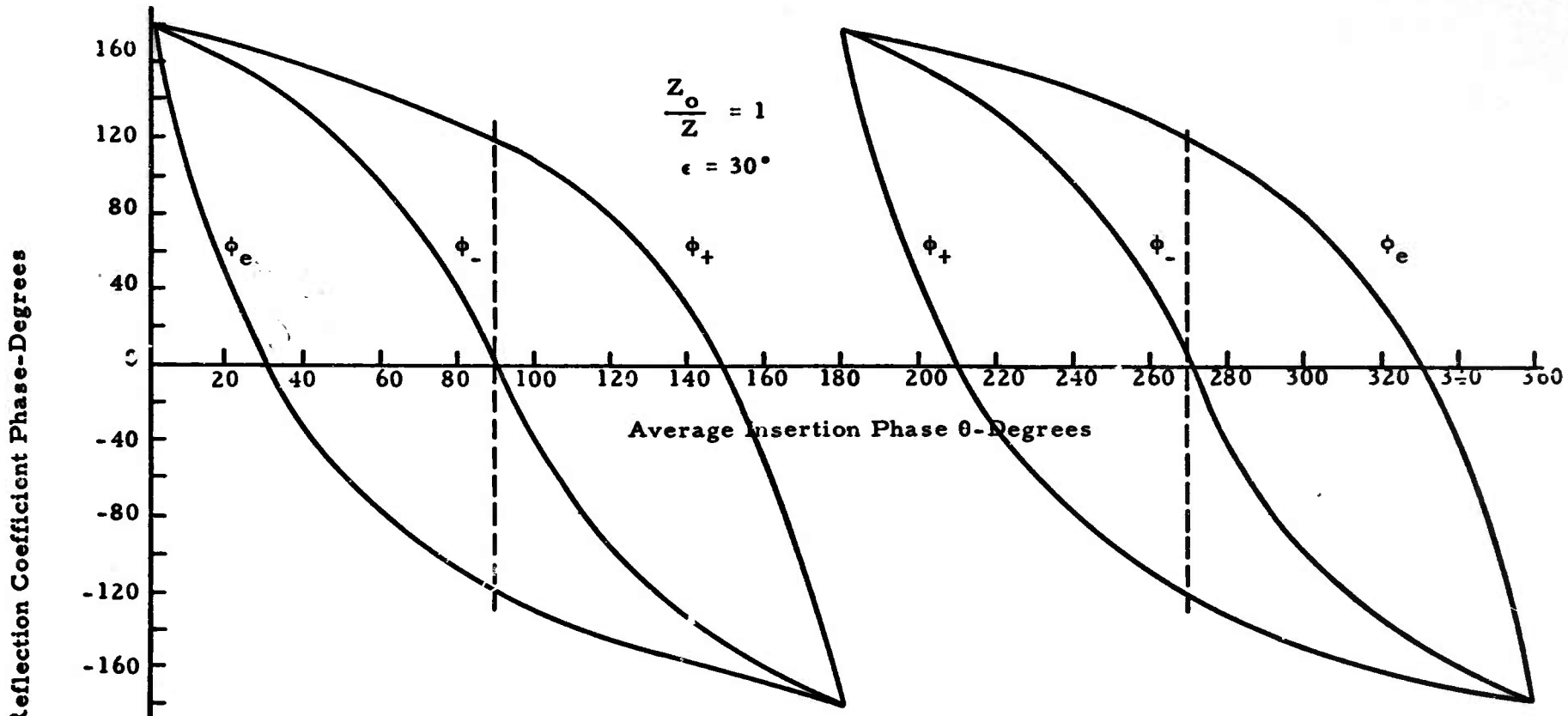

Figure 16. Non Reciprocal Circuit with Circulation at θ = 90° and θ = 270°.

the circulation frequency, of the transmission coefficient to the isolated arm. For circulation in the 1-2-3-1 direction $s_2 = s_1 \exp(+j^{2\pi/3})$ and $s_3 = s_1 \exp(-j^{2\pi/3})$. The variation in isolation about the circulation frequency ω_o is

$$\delta S_{31} = \frac{1}{3} \frac{d}{d\omega} \left[s_1 + e^{j\gamma} s_2 + e^{-j\gamma} s_3 \right] \Bigg|_{\substack{\delta\omega \\ \omega = \omega_o}} \qquad (28)$$

For $S_i = e^{j\phi i}$ $\quad i = 1, 2, 3$ (e, +, - modes)

$$\delta S_{31} = \frac{j}{3} \sum_{i=1}^{3} \frac{d\phi_i}{d\omega} \Bigg|_{\substack{\delta\omega \\ \omega_o}}$$

After some manipulation the magnitude is (equation 29)

$$\left|\delta S_{31}\right| = \frac{1}{3} \left[\sum_{i=1}^{3} \left(\frac{d\phi_i}{d\omega}\right)^2 - \left(\frac{d\phi_1}{d\omega} \frac{d\phi_2}{d\omega} + \frac{d\phi_1}{d\omega} \frac{d\phi_3}{d\omega} + \frac{d\phi_2}{d\omega} \frac{d\phi_3}{d\omega} \right) \right]^{\frac{1}{2}} \Big|_{\omega_o} \delta\omega \Big|$$

It is informative to write the derivatives with respect to ω as

$$\frac{d\phi_i}{d\omega} = \frac{d\phi_i}{d\theta} \frac{d\theta}{d\omega} \qquad i = 1, 2, 3$$

$$= K_i \frac{d\theta}{d\omega}$$

where K_i is just the slope of the reflection coefficient in Figure 16. It may also be determined by taking the derivative of Equations (25-27)

$$K_1 = \frac{-4 \frac{Z_o}{Z} \left(1 + \left[\frac{\cos\theta - \cos\epsilon}{\sin\theta} \right] \cot\theta \right)}{1 + \left(\frac{2Z_o}{Z} \left[\frac{\cos\theta + \sin(30° + \epsilon)}{\sin\theta} \right] \right)^2} \qquad (30)$$

$$K_2 = \frac{-4 \frac{Z_o}{Z} \left(1 + \left[\frac{\cos\theta + \sin(30° + \epsilon)}{\sin\theta} \right] \cot\theta \right)}{1 + \left(\frac{2Z_o}{Z} \left[\frac{\cos\theta + \sin(30° + \epsilon)}{\sin\theta} \right] \right)^2} \qquad (31)$$

$$K_3 = \frac{-4\frac{Z_o}{Z}\left(1 + \left[\frac{\cos\theta + \sin(30 - \epsilon)}{\sin\theta}\right]\cot\theta\right)}{1 + \left(\frac{2Z_o}{Z}\left[\frac{\cos\theta + \sin(30 - \epsilon)}{\sin\theta}\right]\right)^2} \qquad (32)$$

For the circulation condition with 60° differential phase shift ($\epsilon = 30°$), $Z_o = 50$ ohms and the phase shifter an odd number of quarter wavelengths long ($\theta = (2n + 1)\pi/2$)

$$K_1 = K_2 = -1 \qquad K_3 = -4$$

and Equation (29) becomes

$$|\delta S_{31}| = \left|\frac{d\theta}{d\omega}\right|_{\omega_o} \cdot |\delta\omega|$$

and the fractional bandwidth BW for a given isolation is

$$BW = 2\left|\frac{\delta\omega}{\omega_o}\right| = \frac{2|\delta S_{31}|}{\omega_o\left|\frac{d\theta}{d\omega}\right|_{\omega_o}} \qquad (33)$$

The value of θ, the electrical length of the phase shifter, is determined by the percentage of interaction P in the phase shifter.

$$P = \frac{\text{non-reciprocal phase shift}}{\text{average insertion phase}}$$

Sixty degrees non-reciprocal phase shift is required and the lower the interaction the larger θ and hence $\left|\frac{d\theta}{d\omega}\right|$. Bandwidth is inversely proportional to this quantity.

3.3 Circulator Design and Evaluation

A microstrip ring circulator was designed from the graph in Figure 16. The circulator is shown in Figure 17. The phase data for the five section meander line is plotted in Figure 18. Non reciprocal phase ($\Delta\theta$) greater than the required 60° was obtained. The impedance level of the ring was approximately 50 ohms and it had a 1 db insertion loss. The key to the dimensions on the chart is:

b = ground plane spacing
W_e = conductor width of uncoupled lines
W_c = conductor width of coupled lines
s = spacing between coupled lines
ℓ = length of coupled line sections

There were three frequencies in S-Band at which the device circulated. These were where the phase shifter was an odd number of quarter wavelengths long. A typical circulation characteristic is shown in Figure 19. The 20 db isolation bandwidths is 1-1/2 %.

Let us now examine the theoretical bandwidth using Equation 33. For a 20 db isolation bandwidth the formula is

$$BW = \frac{0.2}{\omega_o \left|\frac{d\theta}{d\omega}\right|_{\omega = \omega_o}}$$

From Figure 18, $\frac{d\theta}{d\omega} \approx 420°/\text{GHz}$. The circulation frequency fo is 2.4 GHz. The calculated bandwidth is approximately 1% or 24 MHz which is in good agreement with the experimental value of 36 MHz. The factors causing this narrow bandwidth are (1) the dispersion in the phase shifter and (2) the low interaction (non-reciprocal phase shift/average insertion phase). Both these factors increase $\frac{d\theta}{d\omega}$ and therefore the bandwidth.

Numerous other meander line configurations were designed and

SPL 459

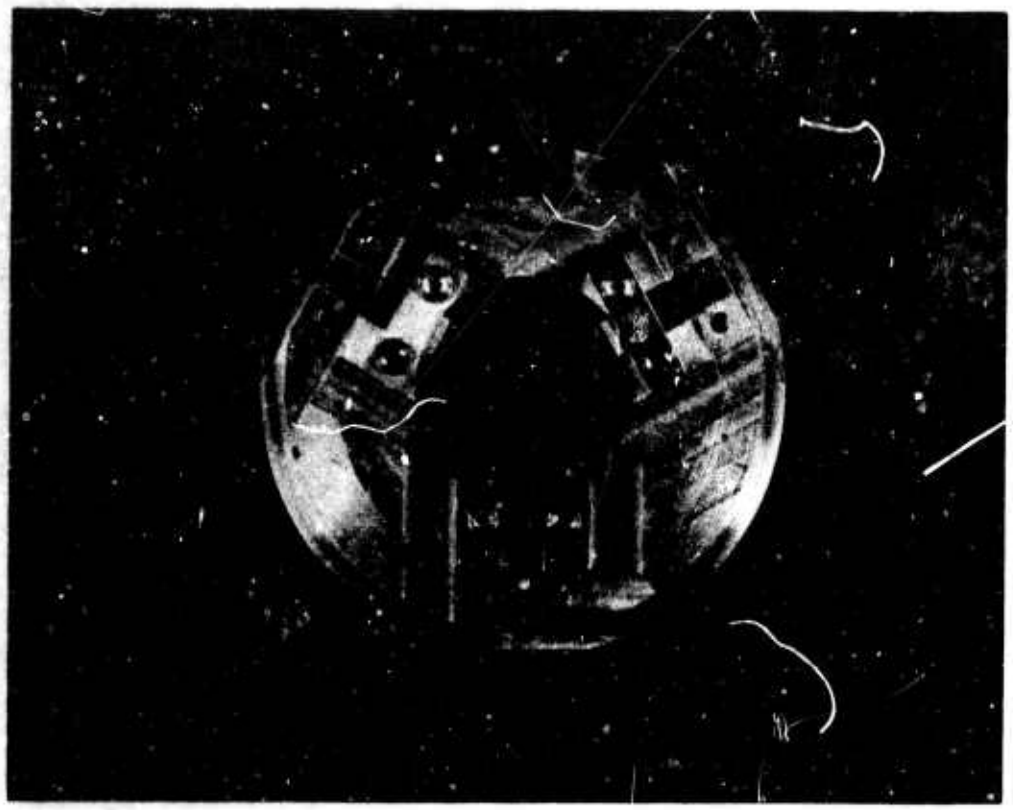

Figure 17. Microstrip Three-Port Ring Circulator with Meander-Line Phase-Shifters

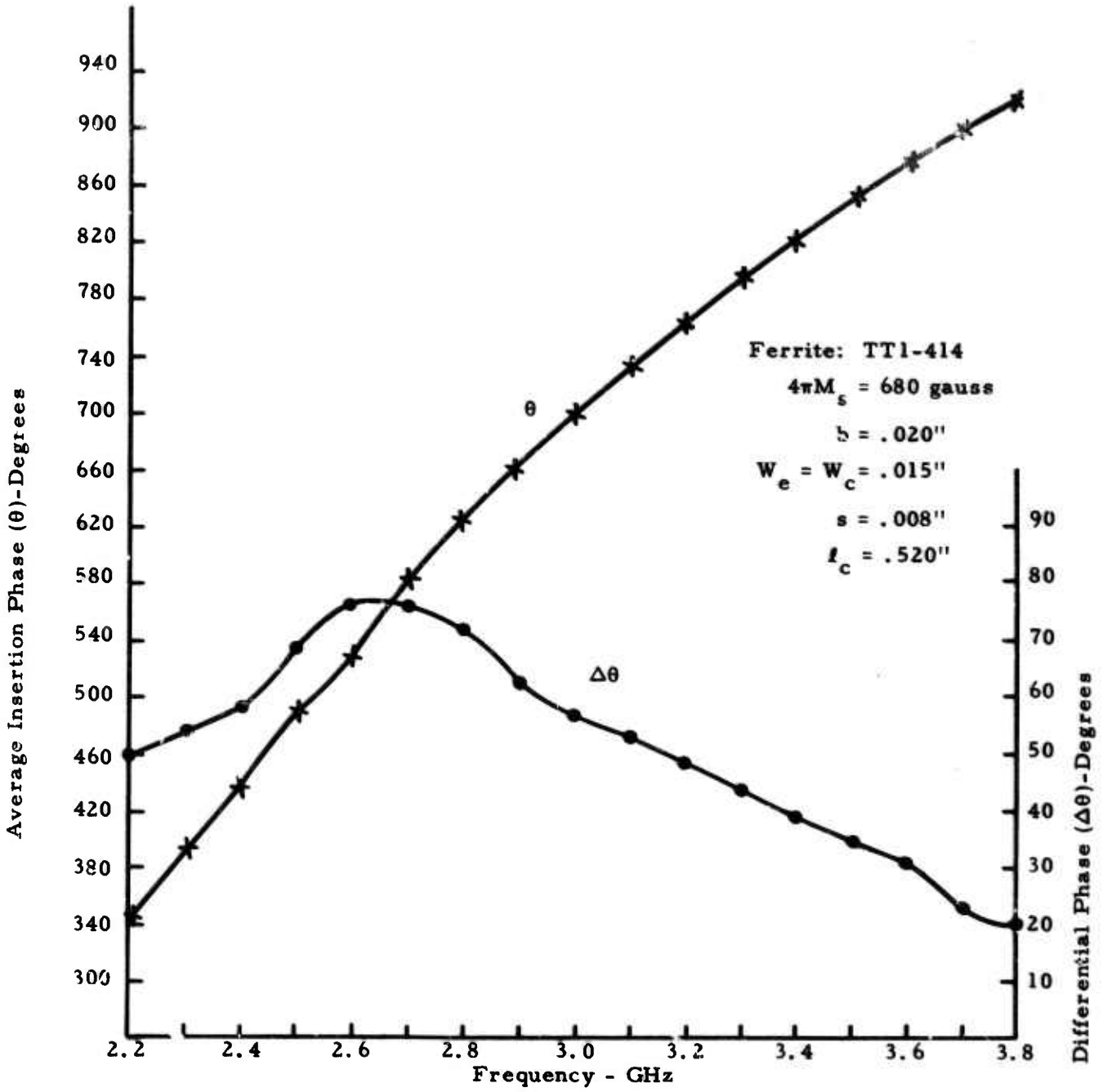

Figure 18. Phase Characteristics for the 5-Line Meander Line Phase-Shifter

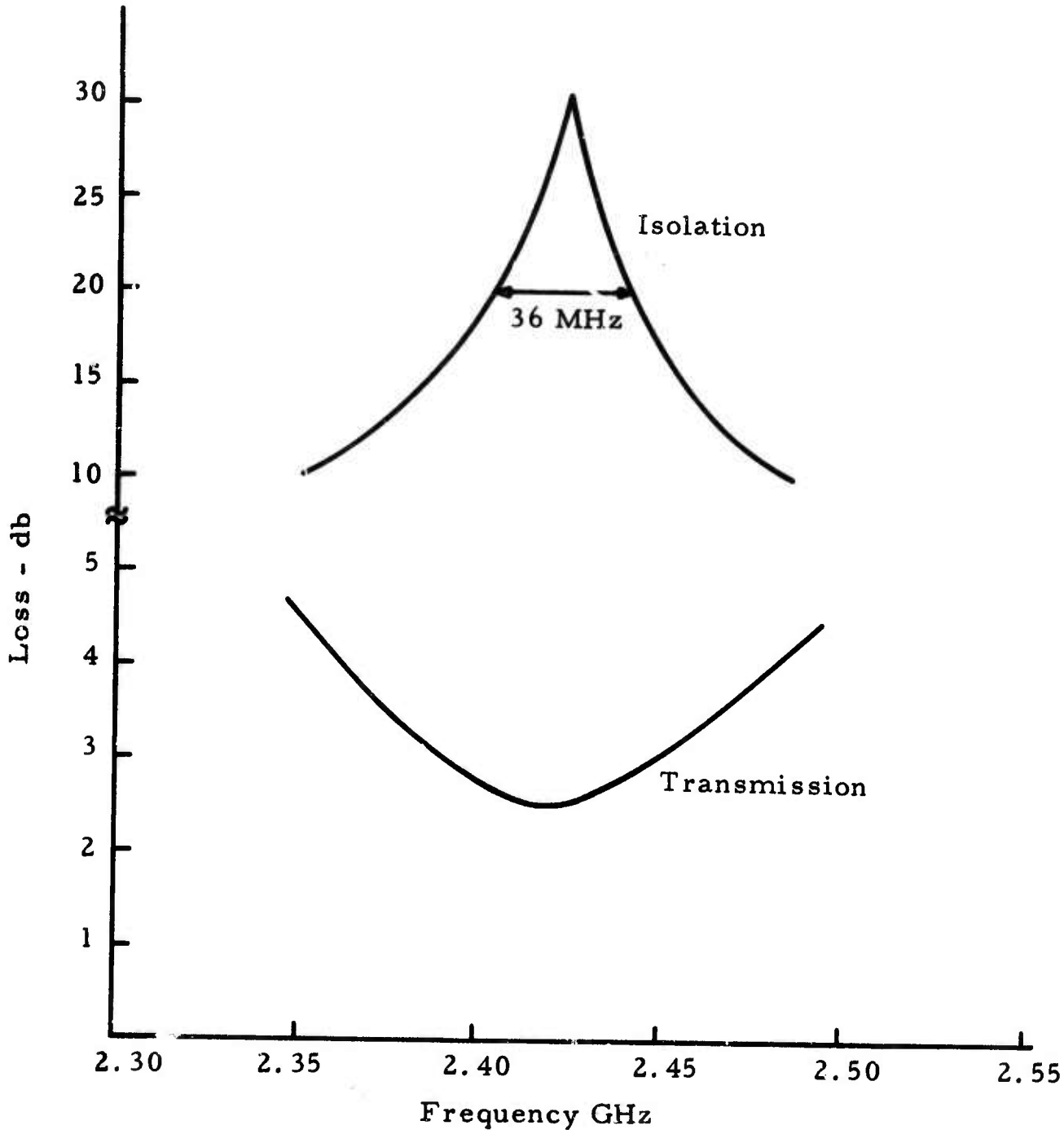

Figure 19. Performance of 5-Line Meander Line Ring Circulator

tested. The coupling, the coupled line lengths, and the number of sections were all varied. No significant improvement in circulation bandwidth was obtained. Because of the large insertion phase required in the actual device, the ring circulator is a high Q narrow bandwidth device.

SECTION 4

THE INVESTIGATION OF THIN DIELECTRIC FILMS FOR MICROWAVE INTEGRATED CIRCUITS

4.1 Introduction

Microwave integrated circuit technology has reduced the cost, weight and size of most components and subsystems used in microwave signal processing. The advent of this technology is leading to the realization of complex electronically steerable array radars with their numerous components and the miniaturization of tactical radar systems. The purpose of this additional effort on Contract F 30 602-67-C-0378 was to investigate a suitable technique for the deposition of the proper dielectric materials which could be used in the design of compatible matching networks for microwave integrated circuits.

Since conventional matching structures are limited by large size and frequency sensitivity, lumped capacitor elements are of critical importance. The characteristics of a capacitor are primarily governed by the intrinsic properties of the dielectric film.

The emphasis of this program has been the selection of a process which will lead to the formation of films with the desired bulk properties. It is also necessary that this technique be compatible with the processes required for the placement of the other microwave components on a common substrate.

4.2 Selection of Deposition Technique

The basic configuration for a thin film capacitor is shown in Figure 20. It consists of a base electrode, a dielectric layer and a counter-electrode. The electrodes are deposited either by vacuum evaporation or sputtering and then electroplated to obtain the required thickness if necessary. The pattern is defined either by masking or by a photo resist process and selective etching. The dielectric layer may be prepared by many different techniques. The four principle methods are vacuum evaporation, sputtering, oxidation, and chem-

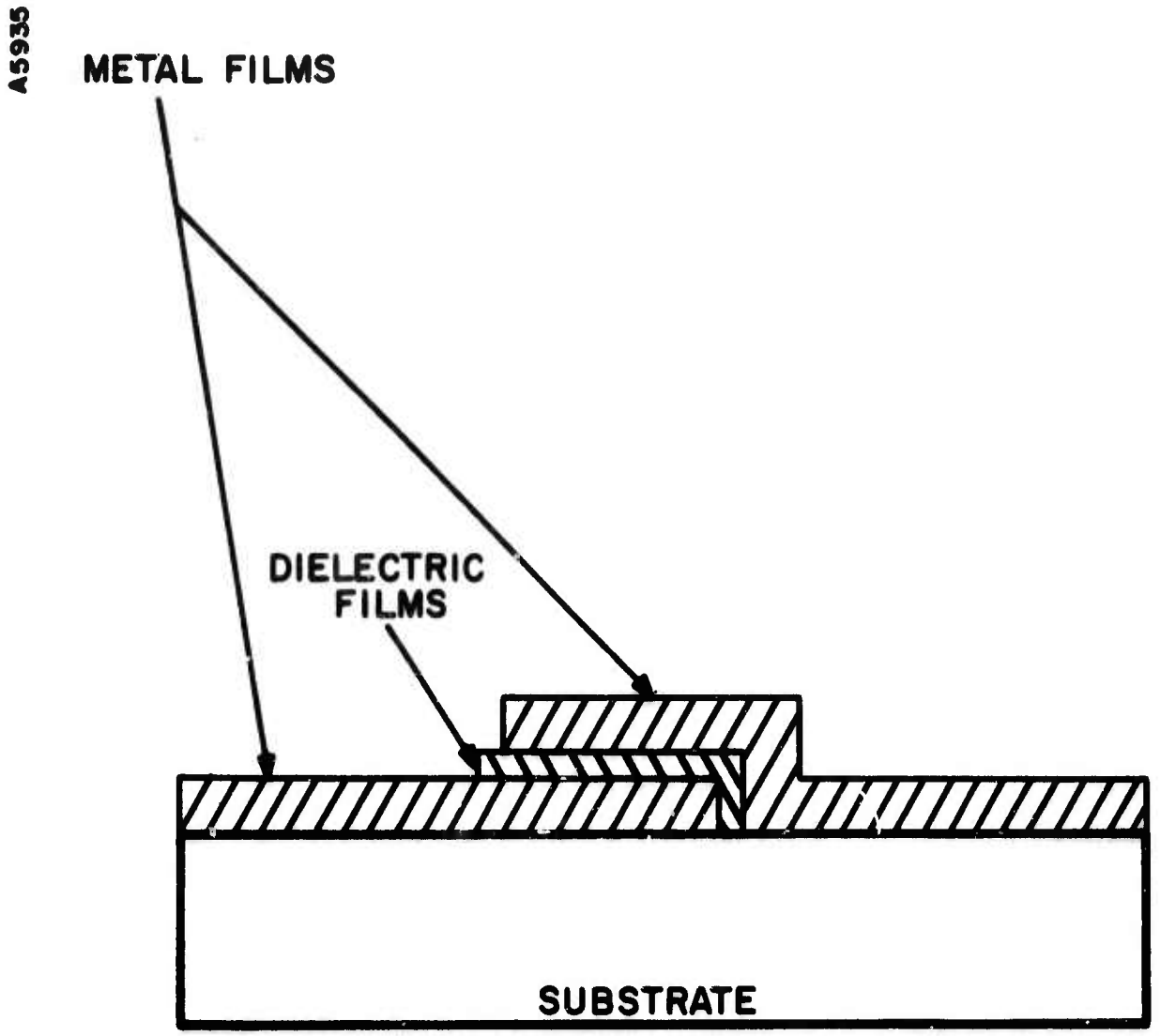

Figure 20. Typical Thin Film Capacitor Construction

ical gas-phase deposition. The applicability of a particular technique depends on the film material and its application. After a careful review of these techniques it appears that at the present time the RF sputtering process is the logical choice because of its compatibility with other microwave integrated circuit techniques and its ability to produce dielectric films with the needed high quality.

4.3 RF Sputtering Process

Sputtering is a process which involves maintaining an inert gas discharge at a pressure between 10^{-4} to 10^{-1} Torr. The source material is negatively biased and thus being bombarded by the positively charged gas ions. When the positive ions strike the target surface their momentum is transferred to the surface atoms of the target. With enough momentum gained, the surface atoms, or group of atoms, of the target will be ejected and thus be deposited on a substrate which is generally located at the anode and in a parallel position to the target. Because sputtering is a momentum-transfer process, high-melting-point materials such as refactory metals and ceramics can be conveniently sputtered. However, if the target is a dielectric material, some means must be provided to neutralize the positive charge accumulation because it will prevent further bombardment by the positively charged gas ions. The most simple way to solve this problem is by placing the dielectric target on the face of an electrode excited by radio-frequency high voltage. The positive surface charge can thus be neutralized on the negative half cycle. Another advantage of this method is that the high electron mobility comparing to the ion mobility produces a negative bias on the surface of the dielectric target so that positively charged gas ions bombard the target only. The radio-frequency used is generally to be 13.56 MHz because it is approved by the FCC for use in industrial applications.

4.4 Experimental Results

An RF sputtering module was designed and constructed at SURC particularly for this work. This module can accommodate a 4-in diameter target. The RF power supply was a modified radio transmitter which operated at

13.56 MHz to comply with the FCC regulations. The RF power supply could deliver a maximum output of about 2.5 KW. During the early stage of this work, this module was used to deposit quartz films. However, due to an intermittent leak developed in the module the results obtained were not consistent. This problem was rectified when a commercially made RF sputtering module (Model SM-8500 manufactured by Material Research Corporation) was available on the market and one unit was purchased and installed in June. A close-up view of this RF sputtering module is shown in Figure 21.

The complete sputtering system in shown in Figure 22 and a schematic of the system is shown in Figure 23. The pumping system consists of a 4-in. oil diffusion pump and a 15-CFM mechanical pump. A matching network was inserted between the RF power supply and the sputtering module for effective coupling. Tuning the sputtering module with varying gas flow and temperature was a tedious task. However, with proper tuning only about 15% of the RF power was being reflected from the sputtering module as indicated by the standing-wave-ratio meter. The biasing capacitor which appeared in Figure 23 was not necessary for sputtering of dielectric films but it must be inserted for sputtering metal films. The high purity quartz sputtering electrode was obtained from Material Research Corporation in the form of a disk 5" in diameter and 1/4" in thickness. The quartz electrode was attached to aluminum backing plate with a silver-based epoxy. Conventional 1" x 3" microscope glass slides were used as substrated. Both the source and the substrate holder were water-cooled during deposition. The source to substrate distance was 1 3/8". The argon pressure during deposition was maintained at 9×10^{-3} Torr by adjusting both the gas leak value and the throttle valve of the pumping system. The pressure was measured by a Pirani gauge. The actual RF power feeding the sputtering module was not measured but an indirect estimation showed that the RF power consumed the sputtering module was about 800W. With the aforementioned deposition parameters the deposition rate was determined to be about 250 Å/min by depositing a series of films with different deposition time and measuring the thickness of the films. A standard multiple beam interferometric method was used to determine the film thickness. The results are shown

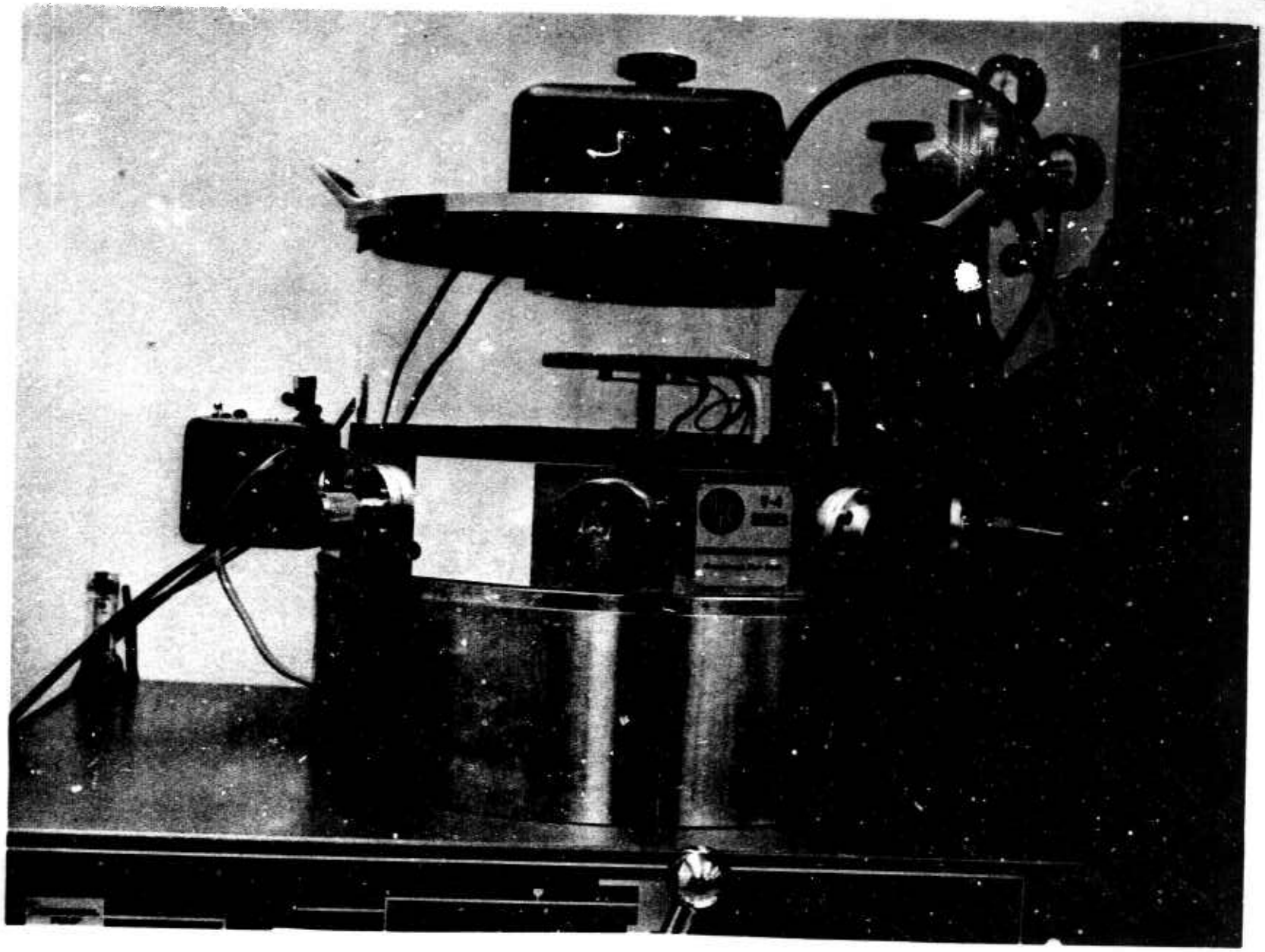

Figure 21 : MRC RF Sputtering Module

A5730

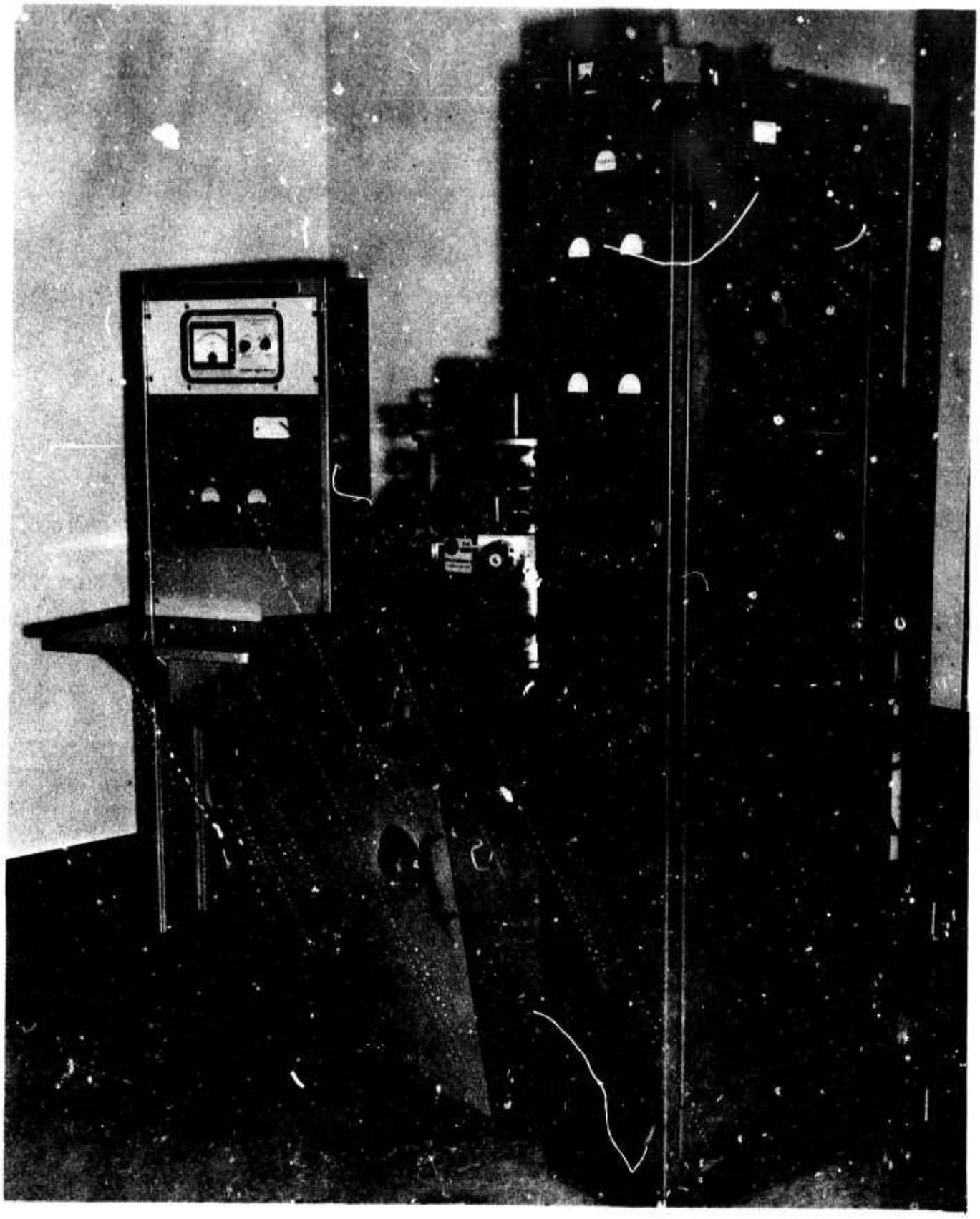

Figure 22 R. F. Sputtering System.

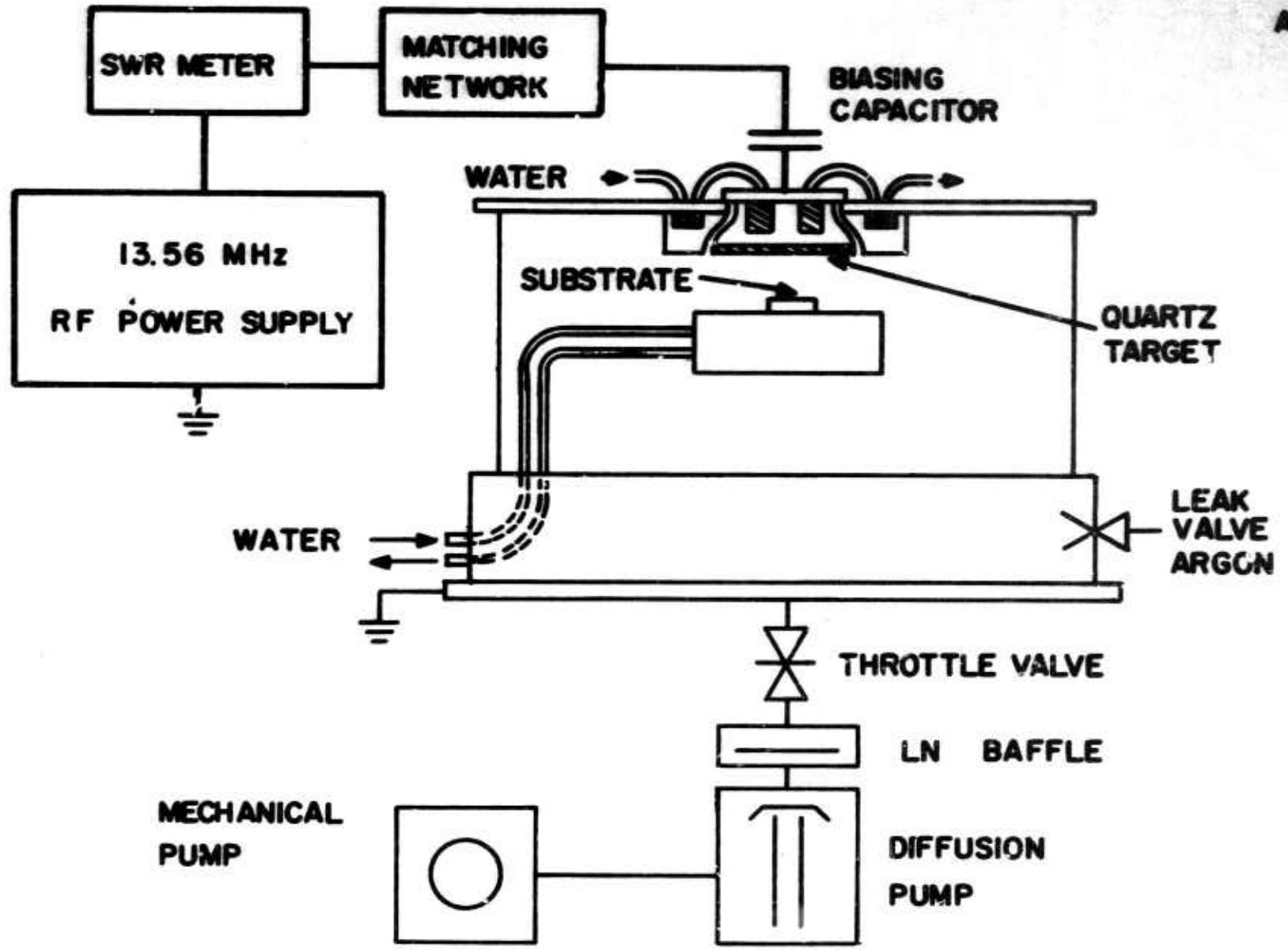

Figure 23 Schematic Drawing of the RF Sputtering System.

in Figure 24.

RF sputtered quartz films were extremely smooth and showed excellent adhesion to the glass substrates. Films up to several microns thick were completely colorless and transparent. The resistivity was extremely high and no meaningful measurement could be made. The results indicated that RF sputtered quartz films are suitable for thin film capacitors.

4.5 Application of RF sputtered Dielectric Films

To form a capacitor, electrodes must be added to the dielectric layer. A typical process for making a thin film capacitor on ferrite substrate may appear as follows (with reference to Figure 25).

1. Successively evaporate or sputter a very thin film of chromium (about 100 Å) and a gold film of several thousand Angstroms thick onto ferrite substrate.
2. Electroplate with fold to a thickness of several skin depths at the frequency range of microwave operation.
3. Define the capacitor pattern by photo resist process and selective etching.
4. Deposit a quartz layer by RF sputtering at selective area using masking technique.
5. Evaporate a chromium-gold film of about one micron thick at the selected area to form the top electrode of the capacitor.

An alternative configuration for a thin film capacitor with a floating top electrode is shown in Figure 26.

Due to the limited funds available for this program it was not possible to fabricate thin film capacitors with various geometry and to pursue extensive tests on the microwave properties of these capacitors.

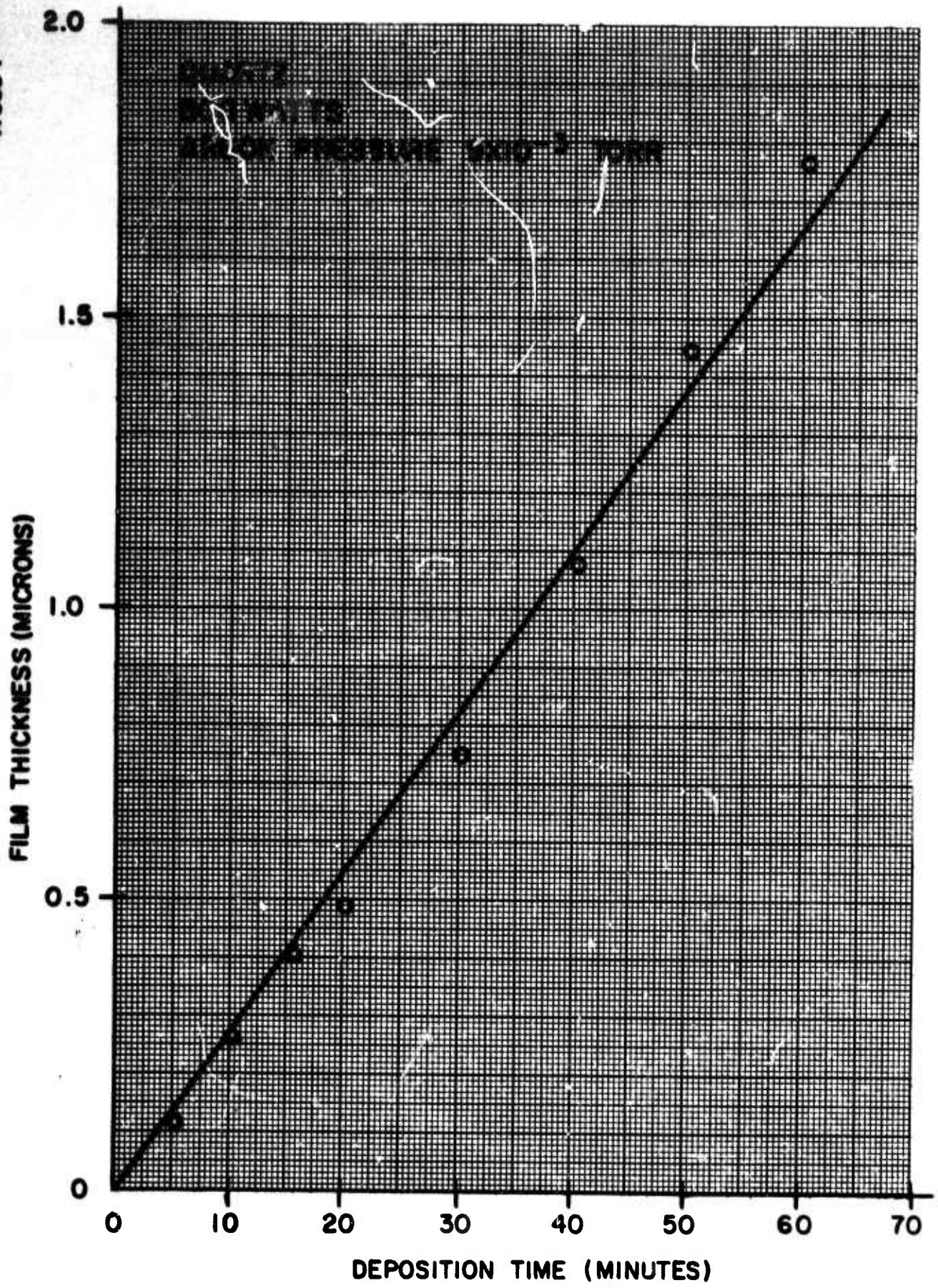

Figure 24 Deposition Data.

A5936

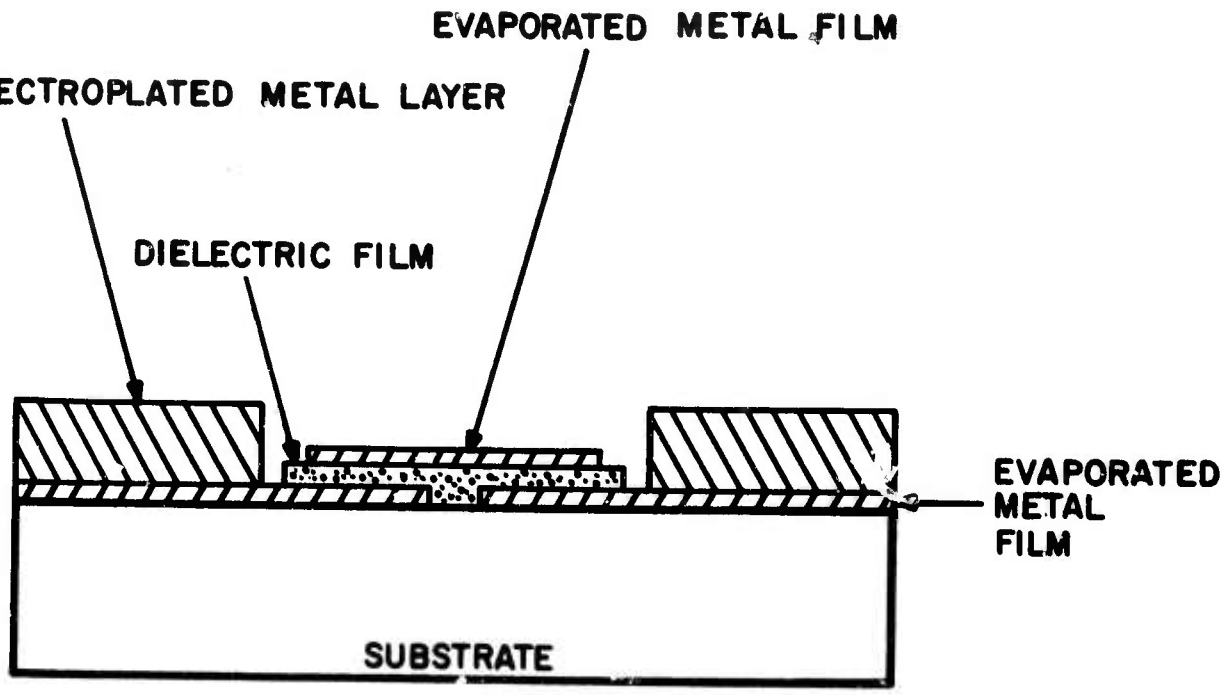

Figure 25. An Alternative Thin Film Capacitor Construction

A5937

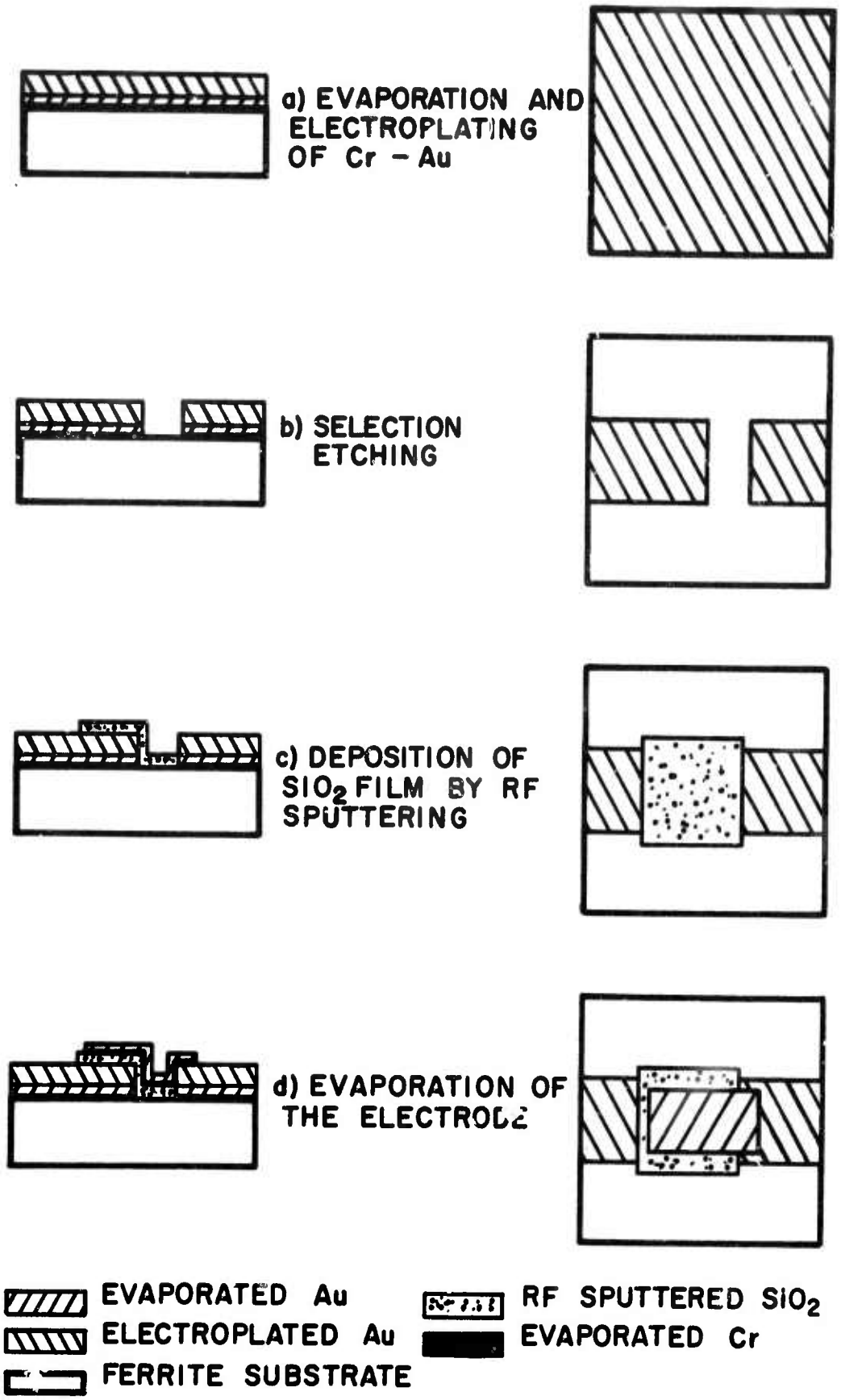

Figure 26. Fabrication Process for Thin-Film Capacitors

SECTION 5

ACKNOWLEDGEMENTS

We wish to acknowledge the Rome Air Development Center for their support and technical assistance during the course of this development program. We also want to thank Messrs. Hugh Hair, Carl Gerst, Chih-Shun Lu, and Gerard Roome for the helpful suggestions furnished during the course of this program.

REFERENCES

1. C.R. Boyd, Jr., "Transmission Lines with Gyromagnetic Coupling," Doctoral Dissertation, Syracuse University, February 1964.

2. C.R. Boyd, Jr., "A Network Model for Transmission Lines with Gyromagnetic Coupling," IEEE Transactions on Microwave Theory and Techniques, Vol. MTT-13, September 1965, pp 652-62.

3. E.M.T. Jones, et.al., "A Nonreciprocal TEM Mode Structure for Wideband Gyrator and Isolator Applications, IRE Transactions on Microwave Theory and Techniques, Vol. MTT-7, October 1959, pp 453-60.

4. Matthaei, et.al., "Microwave Filters, Impedance Matching Networks, and Coupling Structures," McGraw-Hill, 1964, chapter 13.

5. P.C. Goodman, C.R. Tresselt, "S-Band Latching Circulator with 10-Nanosecond Switching Speed," 1967 G-MTT Symposium Digest, pp 73-76.

6. P.C. Goodman, "A Wideband Stripline Match Power Divider," 1968 G-MTT Symposium Digest, pp 16-20.

UNCLASSIFIED

Security Classification

DOCUMENT CONTROL DATA - R & D

(Security classification of title, body of abstract and indexing annotation must be entered when the overall report is classified)

1. ORIGINATING ACTIVITY *(Corporate author)*
Syracuse University Research Corporation,
Special Projects Laboratory,
Merrill Lane, Syracuse, New York 13210

2a. REPORT SECURITY CLASSIFICATION
UNCLASSIFIED

2b. GROUP

3. REPORT TITLE

STRIPLINE FERRITE DEVICES

4. DESCRIPTIVE NOTES *(Type of report and inclusive dates)*
Final Report

5. AUTHOR(S) *(First name, middle initial, last name)*

Martin Sherman

6. REPORT DATE	7a. TOTAL NO. OF PAGES	7b. NO. OF REFS
30 Jun 68	52	6

8a. CONTRACT OR GRANT NO.	9a. ORIGINATOR'S REPORT NUMBER(S)
F30602-67-C-0378	
b. PROJECT NO.	SPL TR 68-54
c. Order No. 550	9b. OTHER REPORT NO(S) *(Any other numbers that may be assigned this report)*
d.	RADC TR-68-525

10. DISTRIBUTION STATEMENT
This document is subject to special export controls and each transmittal to foreign governments, foreign nationals or representatives thereto may be made only with prior approval of RADC (EMATE), GAFB, NY 13440.

11. SUPPLEMENTARY NOTES	12. SPONSORING MILITARY ACTIVITY
Monitored by Rome Air Development Center (EMATE) Griffiss Air Force Base, New York 13440.	Advanced Research Projects Agency Washington, D.C. 20301.

13. ABSTRACT

A stripline instantaneous wideband nonreciprocal hybrid using ferrite material is described. A simple theory of operation, potential use as a broadband circulator and switch is described. The design and data on a laboratory model operating from 3 GHz to 9 GHz is presented.

The theory and results on a three-port switchable S-band microstrip circulator suitable for microwave integrated circuits is also reported. The circulator had a 2 db insertion loss and a 2% bandwidth. Although the insertion loss could be decreased by more refined etching and polishing techniques, the high Q inherent in this "ring" principle of operation severely limits the bandwidth.

Rf sputtering process to deposit dielectric materials for obtaining thin film capacitors is also described.

DD FORM 1 NOV 65 1473

UNCLASSIFIED

Security Classification

14. KEY WORDS	LINK A		LINK B		LINK C	
	ROLE	WT	ROLE	WT	ROLE	WT
hybrid						
ferrite						
circulator						
stripline						
RF sputtering						